© 2018. Published by The Company of Biologists Ltd | Journal of Cell Science (2018) 131, jcs221218. doi:10.1242/jcs.221218

RESEARCH ARTICLE

Gli2 modulates cell cycle re-entry through autophagy-mediated regulation of the length of primary cilia

Ching-Ju Hsiao[1,*], Chia-Hsiang Chang[1,2,*], Ridwan Babatunde Ibrahim[1,3], I-Hsuan Lin[2,4], Chun-Hung Wang[1], Won-Jing Wang[4] and Jin-Wu Tsai[1,5,‡]

ABSTRACT

The primary cilium is a tiny cell protrusion known to transduce key extracellular signals, including those of the sonic hedgehog pathway, which activates Gli transcription factors for various cellular functions. To understand the significance of the Gli2 transcription factor in fibroblasts, we establish a Gli2-knockout NIH3T3 cell line by CRISPR/Cas9 technology. Surprisingly, NIH3T3 fibroblasts lacking Gli2 expression through gene knockout or RNA interference possess longer primary cilia after stimulation of ciliogenesis by serum starvation. This lengthening of primary cilia is associated with enhanced autophagy-mediated Ofd1 degradation, and can be reversed by pharmacological and genetic inhibition of autophagy. Meanwhile, flow cytometry reveals that Gli2$^{-/-}$ NIH3T3 fibroblasts exhibit a delay in cell cycle re-entry after serum re-stimulation. Ablation of their primary cilia through Kif3a knockdown rescues the delay in cell cycle re-entry. These results suggest that Gli2 plays an unexpected role in cell cycle re-entry through an autophagy-mediated regulation on ciliary length in fibroblasts.

KEY WORDS: Gli2, CRISPR/Cas9 technology, Primary cilium, Cell cycle, Autophagy, Ofd1

INTRODUCTION

The primary cilium, consisting of a microtubule-based axoneme, is an antenna-like organelle projecting from a specialized centrosomal structure, the basal body. Although the primary cilium has long been thought to be a vestigial cellular structure since its discovery in 1898 by Zimmerman, its crucial roles in mediating various signaling pathways have emerged in the last decade (Wheatley, 2005), including a role in mediating sonic hedgehog (SHH) signaling. When SHH binds to its receptor Patched-1 (Ptch1), Smoothened (Smo) is released from inhibition and allowed to enter the primary cilium, leading to the activation of Gli transcription factors (Haycraft, 2005). This process is required for many biological processes, such as cell cycle progression, embryonic development, metabolism, tissue homeostasis and tumorigenesis (Tran et al., 2014; Varjosalo and Taipale, 2008). Therefore, disruption of ciliogenesis leads to multiple dysfunction diseases, such as Joubert syndrome, Bardet–Biedl syndrome and Meckel syndrome (Craige et al., 2010; Goetz and Anderson, 2010; Lee and Gleeson, 2011; Waters and Beales, 2011; Williams et al., 2011).

Ciliogenesis is a complex process, beginning with docking of distal appendage proteins to the mother centriole, followed by fusion of ciliary vesicles, formation of transition zone and the extension of microtubule-based axoneme (Graser et al., 2007; Lu et al., 2015; Ott et al., 2018; Szymanska and Johnson, 2012; Tsang et al., 2008; Williams et al., 2011). In fibroblasts, these processes can be initiated by serum starvation, which forces the cells to enter a quiescent (G0) stage. Interestingly, serum starvation not only induces ciliogenesis, but also activates an acute autophagic response (Shang et al., 2011). It has been shown in recent studies that starvation-induced autophagy is required for ciliogenesis; in this process autophagy-related proteins (ATGs) are relocated toward the primary cilium and Ofd1, a key modulator for ciliogenesis and ciliary length, is removed from the centriolar satellites (Pampliega et al., 2013; Tang et al., 2013). In detail, if Hedgehog signaling is enhanced by applying a Smo agonist or overexpressing Gli1, autophagy is increased in a primary cilium-dependent manner (Pampliega et al., 2013). However, another report has shown that Hedgehog signaling impairs the formation of autophagosomes, which relies on the transcription factor Gli2 (Jimenez-Sanchez et al., 2012). Hence, the relationships between Hedgehog signaling, autophagy and ciliogenesis remain elusive.

As Gli2 mediates Hedgehog signaling-induced autophagy, which is important for the induction of ciliogenesis, we postulated that Gli2 may participate in the regulation of ciliogenesis. Thereafter, we utilized CRISPR/Cas9 technology to establish a Gli2$^{-/-}$ cell line for examining the effects on ciliogenesis. Surprisingly, we found that Gli2$^{-/-}$ cells possessed longer primary cilia after serum starvation. Notably, Gli2 depletion enhanced autophagy activity and reduced the Ofd1 protein level. Interestingly, this lengthening of the primary cilium delayed cell cycle re-entry after serum add-back and can be reversed by knocking down Kif3a, a kinesin-II motor protein required for ciliogenesis. Our results demonstrate a novel role for Gli2 that links ciliogenesis, autophagy and the cell cycle.

RESULTS

Generation of Gli2-knockout cells by CRISPR/Cas9 technology

To generate a cell model to study the relationship between Gli2 and primary cilia, we established Gli2$^{-/-}$ cell lines by utilizing CRISPR/Cas9 technology (Doudna and Charpentier, 2014). We constructed three plasmids expressing small guide RNAs (sgRNA) targeting exon 2 of the *Gli2* gene (*Gli2*sgRNA#1, *Gli2*sgRNA#2 and *Gli2*sgRNA#3; Table S1). When these plasmids were each co-

[1]Institute of Brain Science, School of Medicine, National Yang-Ming University, Taipei 112, Taiwan. [2]Taiwan International Graduate Program (TIGP) in Molecular Medicine, National Yang-Ming University and Academia Sinica, Taipei 112, Taiwan. [3]Taiwan International Graduate Program (TIGP) in Interdisciplinary Neuroscience, National Yang-Ming University and Academia Sinica, Taipei 112, Taiwan. [4]Institute of Biochemistry and Molecular Biology, College of Life Sciences, National Yang-Ming University, Taipei 112, Taiwan. [5]Brain Research Center (BRC), and Biophotonics and Molecular Imaging Research Center (BMIRC), National Yang-Ming University, Taipei 112, Taiwan.
*These authors contributed equally to this work

‡Author for correspondence (tsaijw@ym.edu.tw)

J.-W.T., 0000-0003-0135-759X

Received 8 June 2018; Accepted 12 November 2018

Journal of Cell Science (2018) 131, jcs221218. doi:10.1242/jcs.221218

transfected with Cas9 cDNA, they reduced Gli2 protein level in NIH3T3 cells, with *Gli2*sgRNA#1 showing the highest efficiency (Fig. S1A). Thus, we used *Gli2*sgRNA#1 to create Gli2-knockout cells and identified four candidate clones (#2-8, #2-10, #3-11, and #4-27) that showed alterations in DNA sequences in exon2 (Fig. S1B). Among them, clone #4-27 represented the lowest query cover (10%, Table S2) and lowest Gli activity, as determined with a luciferase reporter assay (Fig. S1C). By utilizing TA cloning to separate each allele in clone #4-27, we found that one *Gli2* allele has a deletion of 11 bp (six colonies) while the other has a 5 bp deletion (four colonies) at the sgRNA-targeted sites of exon 2 (Fig. 1A), leading to frameshift mutations. Western blot showed that Gli2 expression in these cells was undetectable (Fig. 1B). To confirm the specificity of Gli2 knockout in clone #4-27, we transfected Gli2 cDNA and found that the Gli2 protein expression and the Gli-luciferase activity can be rescued (Fig. 1B,C). Thus, we established a Gli2-knockout NIH3T3 cell line (termed NIH3T3$^{Gli2-/-}$) for our study.

Gli2-depleted cells possess longer primary cilia after serum starvation

Next, we examined the effects of Gli2 knockout on primary cilia by immunostaining the cells for the ciliary marker ADP-ribosylation factor-like protein 13B (Arl13b). First, we found that a comparable percentage of NIH3T3^{WT} cells and NIH3T3$^{Gli2-/-}$ cells formed primary cilia after serum starvation for 24 h (Fig. S2A). Interestingly, when we measured the length of each primary cilium, the primary cilia of NIH3T3$^{Gli2-/-}$ cells were ∼40% longer than those of wild-type NIH3T3 cells (NIH3T3^{WT}) (NIH3T3^{WT}=2.5±0.5 µm; NIH3T3$^{Gli2-/-}$=3.5±0.7 µm; mean±s.d.; Fig. 2A). This effect was reversed by expression of GFP–Gli2 in the NIH3T3$^{Gli2-/-}$ cells (NIH3T3$^{Gli2-/-}$+Gli2-GFP=2.0±0.6 µm; Fig. 2A), demonstrating that the change of ciliary length was specific to Gli2 manipulations.

To further confirm this result, we used acetylated α-tubulin as a second ciliary marker and showed longer primary cilia in NIH3T3$^{Gli2-/-}$ cells after serum starvation (NIH3T3^{WT}=1.9±0.4 µm; NIH3T3$^{Gli2-/-}$=2.5±0.4 µm; Fig. 2B). In addition, we

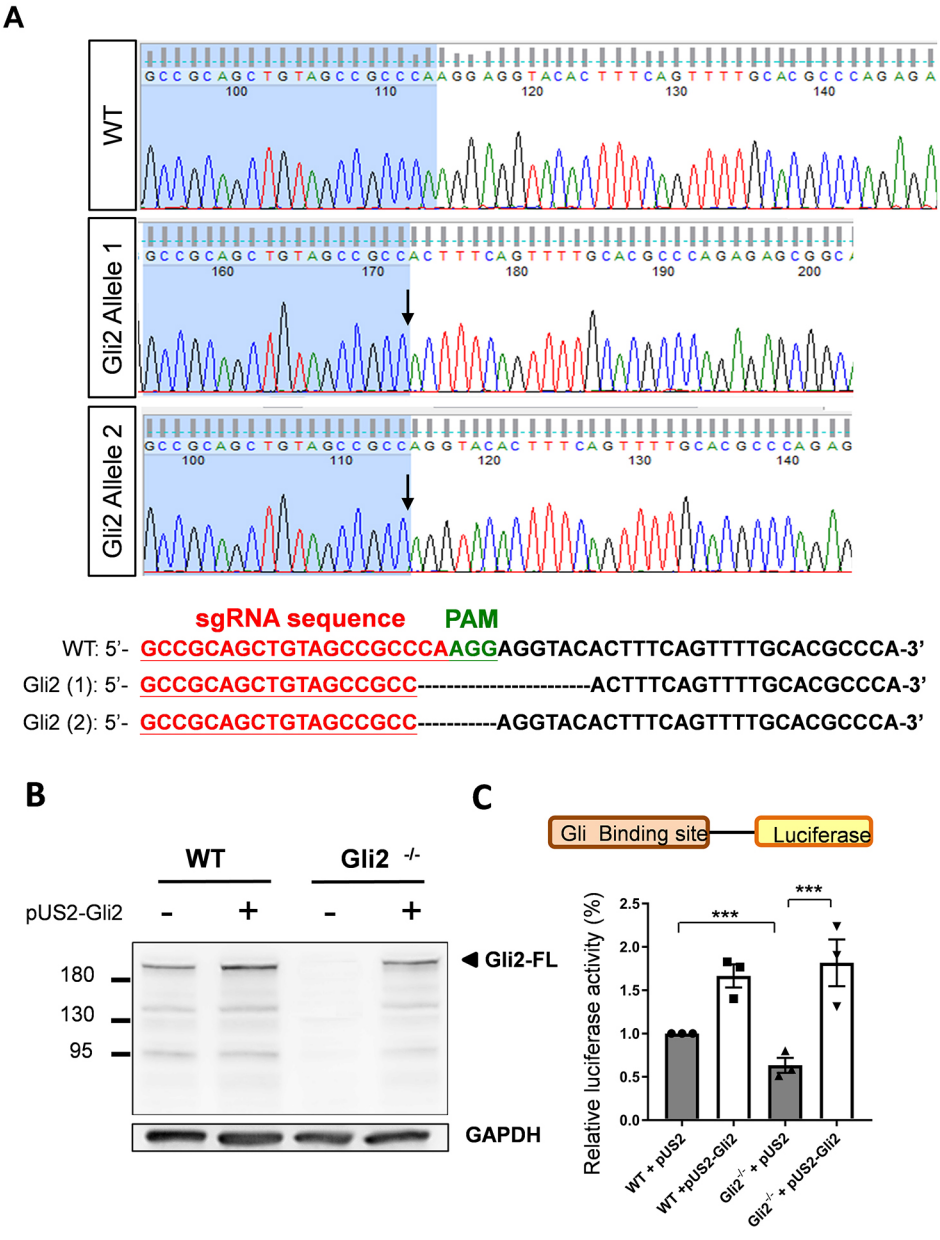

Fig. 1. Generation of Gli2-knockout cells with CRISPR/Cas9 technology. (A) Gli2 sequences of genomic DNA from NIH3T3^{WT} and NIH3T3$^{Gli2-/-}$ cells at the sgRNA-targeted region. Eleven and five nucleotides in the exon 2 regions of the two Gli2 alleles were deleted. Blue box: sgRNA-targeted regions; red letters, sgRNA-targeting sequence; green letters, PAM sequence. Arrows indicate the breaking points. (B) Western blot of Gli2 protein in NIH3T3$^{Gli2-/-}$ and NIH3T3^{WT} cells. Gli2 in NIH3T3$^{Gli2-/-}$ cells was barely detected. Gli2 (full-length, FL) can be restored by transfecting a pUS2-Gli2 construct. GAPDH was immunoblotted as the loading control. (C) Luciferase assay indicating that the binding activity of Gli was significantly decreased in NIH3T3$^{Gli2-/-}$ cells. The Gli-binding activity can be restored after Gli2 overexpression (pUS2-Gli2). The value of Gli–luciferase is normalized to that for *Renilla* luciferase, and further normalized to mutant Gli–luciferase. Bar graph along with individual data points represents the relative value of luciferase activity in each group (n=3 trials). ***P<0.001 (post-hoc Mann–Whitney *U*-test).

Journal of Cell Science (2018) 131, jcs221218. doi:10.1242/jcs.221218

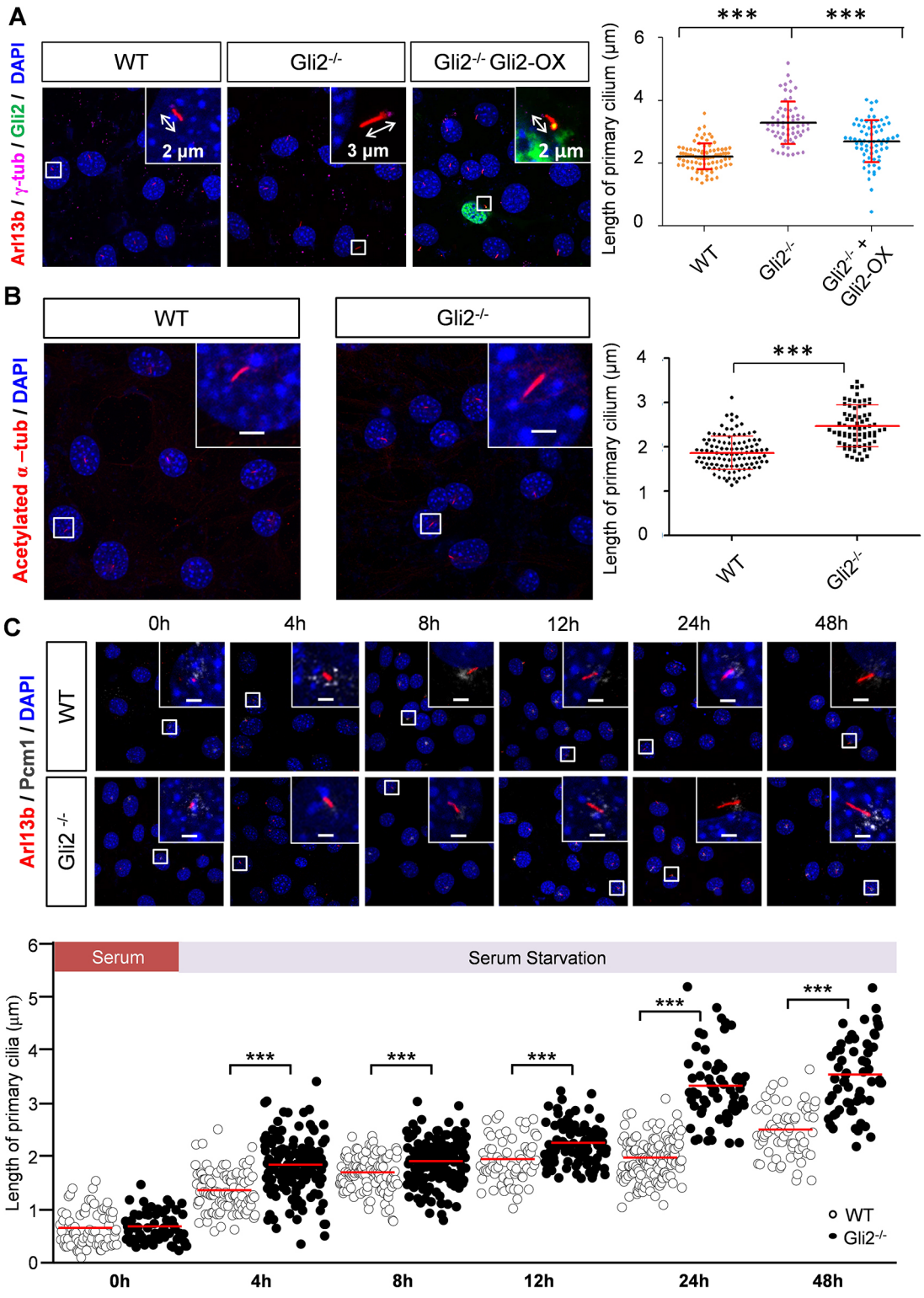

Fig. 2. See next page for legend.

separately applied two short hairpin RNAs (shRNAs) targeting the *Gli2* gene and reduced the Gli2 protein level (Fig. S2B). Cells labeled with Arl13b–GFP again showed longer primary cilia when Gli2 was knocked down (sh-*Gli2*), whereas the primary cilia were moderately shorter when Gli2 was overexpressed (Gli2-OX) (control=3.7±0.2 μm; Gli2-OX=2.6±0.1 μm; sh-*Gli2*#1=5.1±0.3 μm; sh-*Gli2*#2=4.3±0.3 μm; Fig. S2C).

To trace the time course of ciliogenesis in both NIH3T3^{WT} and NIH3T3$^{Gli2-/-}$ cells, we measured the ciliary length from the beginning (0 h after serum starvation, SS 0 h) to an extended period (48 h after serum starvation, SS 48 h). Although the primary cilia of these two cell lines before serum starvation were both short, NIH3T3$^{Gli2-/-}$ cells exhibited longer primary cilia even after an initial 4 h of serum starvation. This effect persisted throughout the

Fig. 2. Longer primary cilia in NIH3T3$^{Gli2-/-}$ cells after serum starvation. (A) Immunofluorescence staining of primary cilia (red, Arl13b), the basal body [magenta, γ-tubulin (γ-tub)] and nucleus (DAPI) in NIH3T3^{WT} and NIH3T3$^{Gli2-/-}$ cells after serum starvation for 24 h. The scatter plot shows that NIH3T3$^{Gli2-/-}$ cells (n=60) possessed longer primary cilia compared to NIH3T3^{WT} cells (n=63), while Gli2 overexpression (OX) (green, GFP-tagged Gli2; n=68) restored the ciliary length in NIH3T3$^{Gli2-/-}$ cells. The bars represent mean±s.d. ***P<0.001 (one-way ANOVA with post-hoc Bonferroni test). (B) Immunofluorescence staining of primary cilia (red, acetylated α-tubulin) and the nucleus (blue, DAPI) in NIH3T3^{WT} and NIH3T3$^{Gli2-/-}$ cells after 24 h of serum starvation. NIH3T3$^{Gli2-/-}$ cells (n=76) possessed longer primary cilia compared to NIH3T3^{WT} (n=110) cells. Scale bars: 2 µm. The bars represent mean±s.d. ***P<0.001 (Student's t-test). (C) Time course of ciliary length in NIH3T3 cells after serum starvation. Immunostaining the primary cilia (red, Arl13b), centriolar satellites (gray, Pcm1) and the nucleus (DAPI) in NIH3T3^{WT} and NIH3T3$^{Gli2-/-}$ cells after serum starvation for 0, 4, 8, 12, 24 and 48 h. The ciliary lengths of NIH3T3$^{Gli2-/-}$ cells were significantly longer than NIH3T3^{WT} after serum starvation for 4, 8, 12, 24 and 48 h. Scale bars: 2 µm. NIH3T3^{WT} at 0 h, n=74; 4 h, n=102; 8 h, n=105; 12 h, n=65; 24 h, n=135; 48 h, n=63; NIH3T3$^{Gli2-/-}$ at 0 h, n=65; 4 h, n=156, 8 h, n=152; 12 h, n=97; 24 h, n=115; 48 h, n=65. ***P<0.001 (Student's t-test). Scatter plot displays individual cilia in NIH3T3^{WT} cells (white circles) and NIH3T3$^{Gli2-/-}$ cells (black dots). Red lines mark the mean.

48 h of serum starvation (Fig. 2C). Interestingly, both NIH3T3^{WT} and NIH3T3$^{Gli2-/-}$ cells showed a similar percentage of ciliated cells throughout the entire course of ciliogenesis even though there was a slight increase in ciliated NIH3T3$^{Gli2-/-}$ cells after 4 h of serum starvation (Fig. S2A). Taken together, these results indicate that manipulation of Gli2 level alters the length of primary cilia after serum deprivation.

Gli2 knockout increased autophagy and Ofd1 removal upon serum starvation

Previously, serum starvation has been shown to not only lead to cell cycle exit, but also triggers autophagy-mediated Ofd1 removal, which is required for ciliary growth (Tang et al., 2013). Hence, we tested whether NIH3T3$^{Gli2-/-}$ cells might have longer primary cilia after serum starvation because of an upregulation of autophagy. We first followed autophagy activities over time after serum starvation by measuring the protein level of the autophagosome marker, the lipdated form of LC3 proteins (also known as MAP1LC3), denoted LC3-II, and the degradation of the autophagy substrate p62 (also known as sequestosome 1, SQSTM1). We found that the protein level of LC3-II was significantly higher in NIH3T3$^{Gli2-/-}$ cells than in NIH3T3^{WT} cells. Consistent with this, NIH3T3$^{Gli2-/-}$ cells also exhibited faster p62 degradation (Fig. 3A), suggesting that the autophagy activity is raised when Gli2 is depleted. When treated with the lysosome inhibitor chloroquine (CQ), NIH3T3$^{Gli2-/-}$ cells still exhibited a higher LC3-II level compared to wild-type cells 4 h after serum starvation (Fig. S3A), suggesting a higher level of autophagy.

We then followed Ofd1 protein level during the whole course of serum starvation. Similar to the course of p62 protein degradation (Sahani et al., 2014), we found that the Ofd1 protein level increased during the first 4–12 h and then decreased at the later stage of serum starvation in wild-type cells (12–48 h, Fig. 3A). Interestingly, the protein level of Ofd1 in NIH3T3$^{Gli2-/-}$ cells was reduced within the first 4 h after serum starvation (Fig. S3B), and then underwent faster degradation at the later stage (12–48 h; Fig. 3A). To examine whether this decreased Ofd1 level reflects a reduction of Ofd1 at the centriolar satellites, we measured Ofd1 intensity specifically around the centrioles by immunostaining 24 h after serum starvation. Consistent with the above results, the Ofd1 intensity surrounding the centrioles was lower in NIH3T3$^{Gli2-/-}$ cells (Fig. S3C), indicating that more Ofd1 is removed from the centriolar satellites in Gli2-depleted cells after serum deprivation for 24 h. Importantly, the increase in autophagy and decrease in Ofd1 in NIH3T3$^{Gli2-/-}$ cells were not observed in serum-rich medium (Fig. S4A), as is also reflected by no difference in the percentage of ciliated cells (Fig. S4B) and ciliary length (Fig. 2C, time zero), indicating that this process is specific to serum starvation-induced ciliogenesis.

The increase in LC3-II protein level may reflect higher autophagic flux or a block of autophagosome–lysosome fusion. To dissect these possibilities, we transfected plasmids encoding RFP–GFP–LC3 in NIH3T3^{WT} and NIH3T3$^{Gli2-/-}$ cells to detect autophagosome–lysosome fusion. Upon the onset of autophagy, RFP–GFP–LC3, which appears yellow, is recruited to autophagosomes. As autophagosomes fuse with lysosomes, GFP fluorescence is quenched under the acidic environment, and thus autolysosomes appear red (Orhon et al., 2016). Interestingly, both the numbers of autophagosomes (yellow) and autolysosomes (red) were higher in NIH3T3$^{Gli2-/-}$ cells than that in NIH3T3^{WT} cells (Fig. 3B,C). Note that the ratio between autolysosome and autophagosomes was not changed in NIH3T3$^{Gli2-/-}$ cells (Fig. 3D), indicating that the elevation of LC3-II in NIH3T3$^{Gli2-/-}$ cells was due to an escalation of autophagic flux and not a blockade between autophagosomes and lysosome fusion. Taken together, we found that the autophagy flux is highly activated in NIH3T3$^{Gli2-/-}$ cells upon serum starvation while basal autophagy is not significantly disturbed.

Gli2 knockout increased ciliary length through autophagy-dependent Ofd1 removal

To investigate whether autophagy is responsible for the increase in ciliary length in NIH3T3$^{Gli2-/-}$ cells, we treated NIH3T3^{WT} and NIH3T3$^{Gli2-/-}$ cells with 3-methyladenine (3-MA), an autophagy inhibitor, during the first 4 h of serum deprivation. Indeed, 3-MA significantly decreased the LC3-II protein levels in both NIH3T3^{WT} and NIH3T3$^{Gli2-/-}$ cells (Fig. 4A). Consistent with this, the protein level of Ofd1 was recovered in NIH3T3$^{Gli2-/-}$ cells treated with 3-MA (Fig. S5A), indicating that 3-MA successfully blocked the autophagy-dependent Ofd1 removal. Remarkably, we found that while Gli2 knockout increased the ciliary length, 3-MA treatment brought the length back to normal in NIH3T3$^{Gli2-/-}$ cells (NIH3T3^{WT}+DMSO=1.87±0.04 µm; NIH3T3$^{Gli2-/-}$+DMSO=2.48±0.05 µm; NIH3T3^{WT}+3-MA=1.49±0.06 µm; NIH3T3$^{Gli2-/-}$+3-MA=1.95±0.06 µm; Fig. 4B), indicating that the elevated autophagic flux during ciliogenesis plays a fundamental role for ciliary elongation in NIH3T3$^{Gli2-/-}$ cells. To further test this possibility, we used shRNA targeting Atg3 along with a GFP reporter (sh-*Atg3*-GFP), an ATG protein crucial for autophagosome formation, as an additional tool to block autophagy (Mizushima and Komatsu, 2011). Cells infected with lentiviruses encoding sh-*Atg3*-GFP had significantly less LC3-II protein compared to the control group (Fig. 4C). Similarly, the primary cilia in NIH3T3$^{Gli2-/-}$ cells had a normal length after sh-*Atg3*-GFP transfection (NIH3T3^{WT}+sh-Ctrl-GFP=2.07±0.04 µm; NIH3T3$^{Gli2-/-}$+sh-Ctrl-GFP=2.77±0.04 µm; NIH3T3^{WT}+sh-*Atg3*-GFP=1.22±0.03 µm; NIH3T3$^{Gli2-/-}$+sh-*Atg3*-GFP=1.78±0.03 µm; Fig. 4D).

To investigate whether autophagy-dependent Ofd1 removal is required downstream of Gli2 depletion for the ciliary lengthening, we transfected NIH3T3^{WT} and NIH3T3$^{Gli2-/-}$ cells with Myc-tagged Ofd1 (pIRES2-Ofd1-Myc) or its control empty vector (pIRES2). After serum starvation for 24 h, Ofd1 overexpression reduced the percentage of ciliated cells as well as the ciliary length in NIH3T3^{WT} cells (Fig. S5B–D), consistent with previous findings (Tang et al., 2013). In NIH3T3$^{Gli2-/-}$ cells, forced expression of

Journal of Cell Science (2018) 131, jcs221218. doi:10.1242/jcs.221218

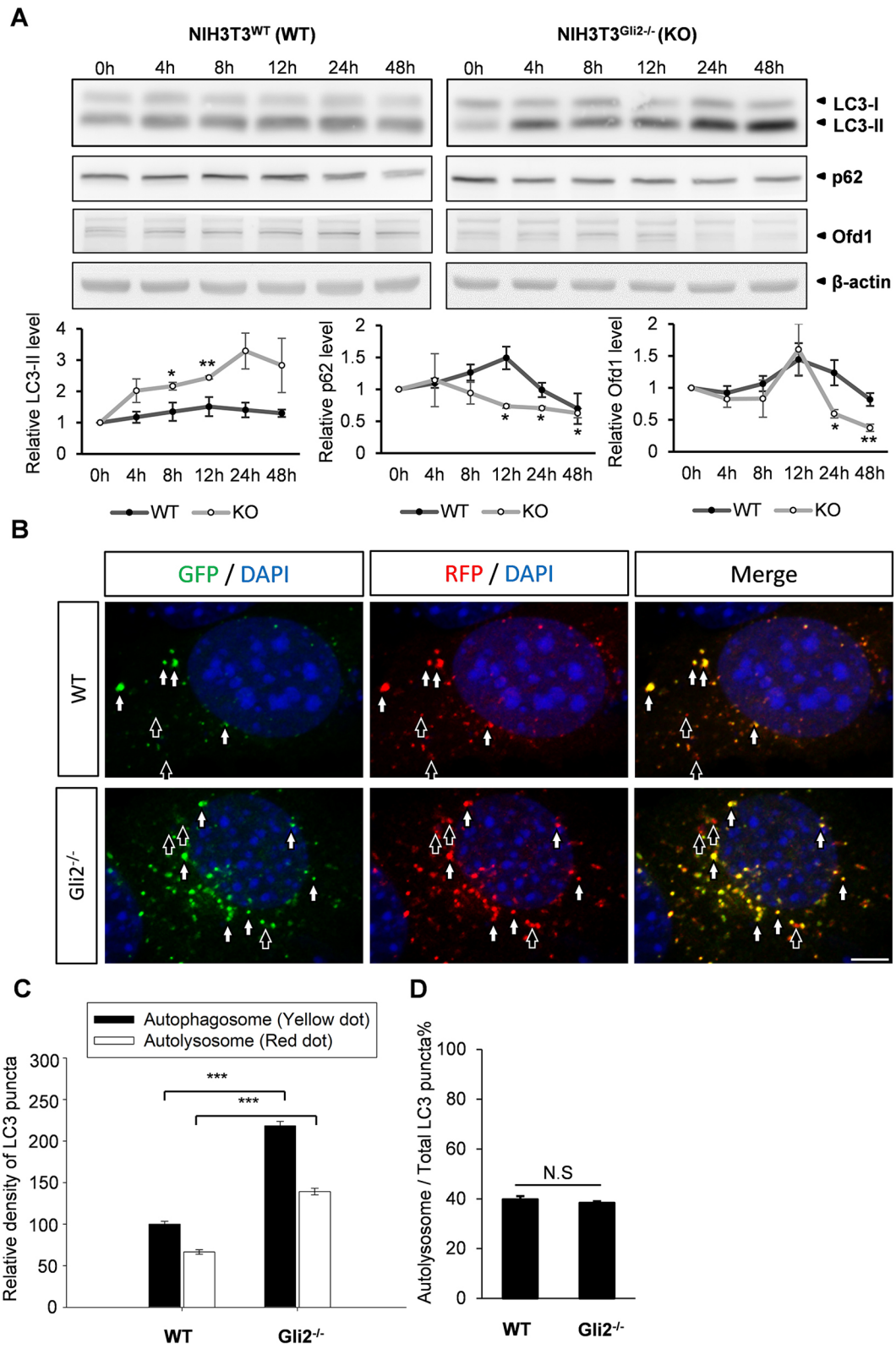

Fig. 3. Increase in autophagic activities in NIH3T3$^{Gli2-/-}$ cells. (A) Protein lysates were collected from NIH3T3^{WT} and NIH3T3$^{Gli2-/-}$ cells after serum starvation (SS) for 0, 4, 8, 12, 24, and 48 h, and immunoblotted for LC3, p62 and Ofd1. β-actin was used as the loading control. Line charts show the relative protein levels of LC3-II (left), p62 (middle) and Ofd1 (right) in NIH3T3$^{Gli2-/-}$ cells (white circles) compared to WT cells (black circles). Results are mean±s.e.m.; n=3, *P<0.05; **P<0.01 (Student's t-test). (B) Autophagosomes and autolysosomes labeled with RFP–GFP–LC3 transfected into NIH3T3^{WT} and NIH3T3$^{Gli2-/-}$ cells. Autophagosomes (white arrows) appear as yellow whereas autolysosomes (black arrows) appear red due to GFP fluorescence being quenched in the acidic environment. Scale bar: 5 µm. (C) Bar graph showing that the relative density of both autophagosome and autolysosome puncta are higher in NIH3T3$^{Gli2-/-}$ cells (n=59 cells) than those in NIH3T3^{WT} cells (n=21 cells). ***P<0.001 (Student's t-test). (D) Bar graph showing that there is no difference in the percentage of autolysosome versus total LC3 puncta between NIH3T3^{WT} and NIH3T3$^{Gli2-/-}$ cells. NS, not significant (Student's t-test). Results in C and D are mean±s.e.m.

Journal of Cell Science (2018) 131, jcs221218. doi:10.1242/jcs.221218

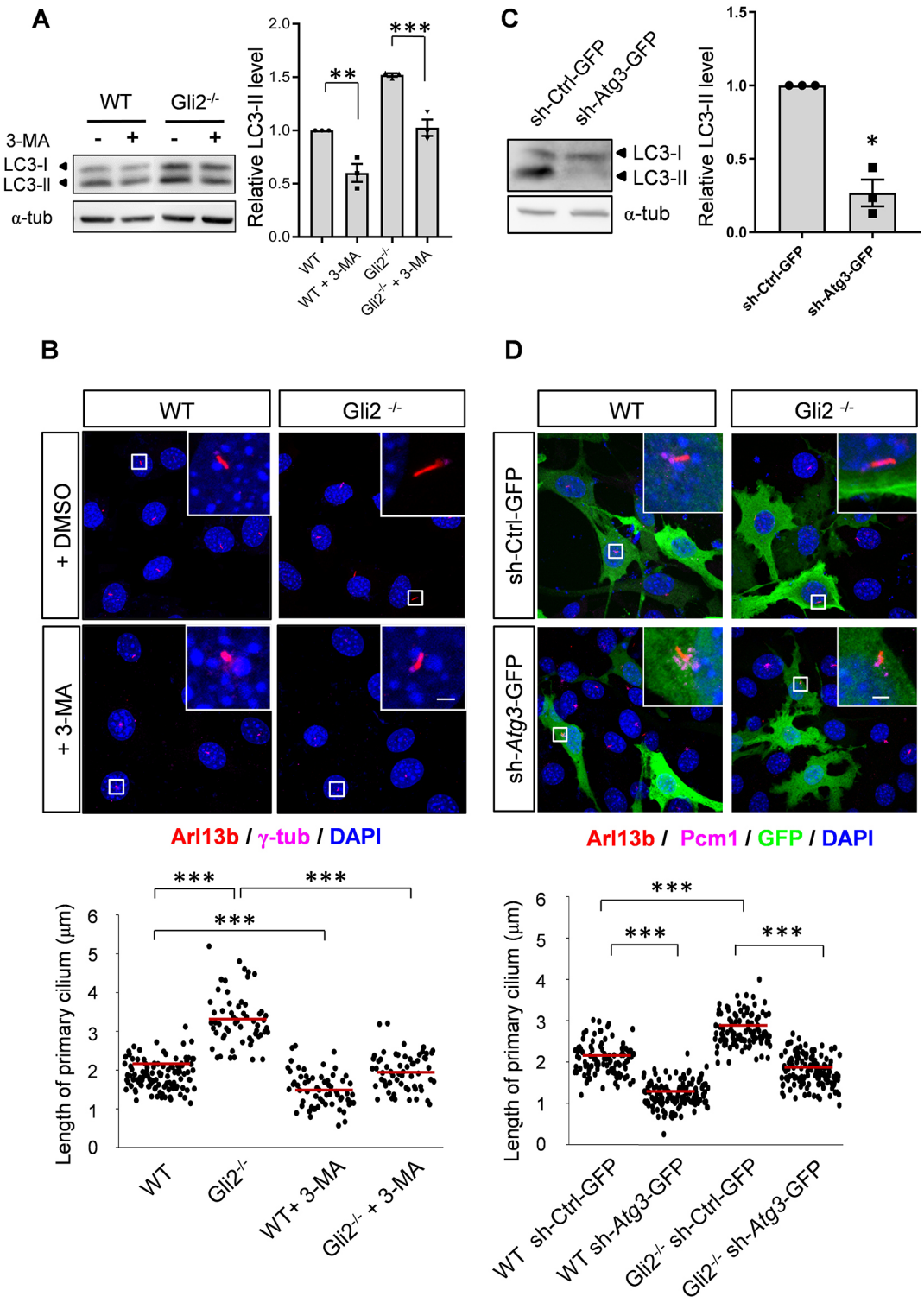

Fig. 4. See next page for legend.

Ofd1 brought the ciliary length back to normal (Fig. S5B,D). Taken together, these results suggest that the activation of autophagy-dependent Ofd1 removal is crucial for the ciliary lengthening in Gli2-knockout cells.

Long cilia delayed cell cycle re-entry in NIH3T3$^{Gli2-/-}$ cells

Typically, primary cilia form at the G0/G1 phase of the cell cycle and undergo disassembly when cells re-enter the cell cycle (Kim and Tsiokas, 2011). In previous reports, a longer primary cilium was shown to be associated with the delay in cell cycle re-entry (Kim et al., 2011). Therefore, we tested whether the elongated primary cilium delayed the process of ciliary resorption and cell cycle re-entry in Gli2-knockout cells by immunostaining and flow cytometry.

NIH3T3^{WT} and NIH3T3$^{Gli2-/-}$ cells were synchronized at the G0 phase after serum starvation for 24 h. By immunostaining for

Journal of Cell Science (2018) 131, jcs221218. doi:10.1242/jcs.221218

Fig. 4. Inhibition of autophagy restores the ciliary length in NIH3T3$^{Gli2-/-}$ cells. (A) Western blot of LC3 in NIH3T3 cells treated with an autophagy inhibitor, 3-methyladenine (3-MA). α-tubulin (α-tub) was immunoblotted as the loading control. Bar graph along with individual data points shows that 3-MA reduced LC3-II expression both in NIH3T3^{WT} and NIH3T3$^{Gli2-/-}$ cells (n=3 trials). **P<0.01, ***P<0.001 (one-way ANOVA with a post-hoc Bonferroni test). (B) Immunofluorescence staining of primary cilia (red, Arl13b), basal body [magenta, γ-tubulin (γ-tub)] and the nucleus (blue, DAPI) in NIH3T3^{WT} and NIH3T3$^{Gli2-/-}$ cells treated with DMSO or 3-MA at the first 4 h of the 24 h serum starvation period. The inset shows the boxed region in each panel. Scale bar: 2 µm. Scatter plots show that primary cilia are longer in NIH3T3$^{Gli2-/-}$ cells (n=60) than NIH3T3^{WT} cells (n=63), while 3-MA significantly reduced the length of primary cilia in both cells (n=61 and 62 in NIH3T3$^{Gli2-/-}$ cells and NIH3T3^{WT} cells, respectively). ***P<0.001 (one-way AVOVA with post-hoc Bonferroni test). The red line indicates the mean. (C) Immunoblots of LC3 in NIH3T3 cells transfected with sh-Ctrl-GFP or sh-*Atg3*-GFP and selected by puromycin treatment. α-tubulin (α-tub) serves as the loading control. Bar graph along with individual data points shows that cells transfected with sh-*Atg3*-GFP exhibited lower LC3-II protein compared to control group upon serum starvation. Results are mean±s.e.m.; n=3 trials. *P<0.05 (Student's t-test). (D) Immunostaining for primary cilia (Arl13b, red), centriolar satellites (Pcm1, magenta) and the nucleus (DAPI, blue) in NIH3T3^{WT} and NIH3T3$^{Gli2-/-}$ cells transfected with sh-Ctrl-GFP or sh-*Atg3*-GFP. Insets show the primary cilia in the boxed regions of each panel. Scale bar: 2 µm. Scatter plots show that primary cilia were longer in NIH3T3$^{Gli2-/-}$ cells (n=105) than in NIH3T3^{WT} cells (n=100), while sh-*Atg3*-GFP reduced the length of primary cilia in both cells (n=133 and 131 in NIH3T3$^{Gli2-/-}$ cells and NIH3T3^{WT} cells, respectively). Red lines mark the mean. ***P<0.001 (one-way AVOVA with post-hoc Bonferroni test).

markers labeling the primary cilium (Arl13b) and centrioles (γ-tubulin), we showed that, in NIH3T3^{WT} cells, the primary cilia were absorbed over time after serum re-stimulation, exhibiting a two-phase decrease both in ciliary length (Fig. 5A) and in the percentage of ciliated cells (Fig. 5B) as previously described (Pugacheva et al., 2007). However, Gli2 depletion slowed down this process, resulting in longer primary cilia and higher percentage of ciliated cells during ciliary resorption phase compared to wild-type cells (Fig. 5A,B).

Finally, by using the flow cytometry to decipher the phases of cell cycle, we found that NIH3T3^{WT} cells progressed to S-G2-M phase over time after serum was added back (Fig. 6B,C). However, the percentage of S-G2-M phase in NIH3T3$^{Gli2-/-}$ cells did not increase as much as NIH3T3^{WT} cells after serum re-stimulation even for 24 h (NIH3T3^{WT}=53.9±1.3%; NIH3T3$^{Gli2-/-}$=39.2±1.0%; mean±s.e.m.; Fig. 6B,C), showing that there was a significant delay in cell cycle re-entry. As NIH3T3^{WT} and NIH3T3$^{Gli2-/-}$ cells possess similar distribution of cells in each phase of the cell cycle under serum-rich conditions (Fig. S6A), we postulated that the delay in cell cycle re-entry in NIH3T3$^{Gli2-/-}$ cells could be caused by the delay in ciliary resorption resulting from an lengthened primary cilium (Fig. 5A). To examine this hypothesis, we disrupted primary cilia by knocking down Kif3a, a kinesis II motor protein required for ciliogenesis. By immunostaining, we showed that applying the sh-*Kif3a*-GFP construct was able to eliminate primary cilia in both NIH3T3^{WT} and NIH3T3$^{Gli2-/-}$ cells despite serum starvation for 24 h (Fig. 6A), consistent with the results in our previous report (Chen et al., 2018). Interestingly, ablating the primary cilium by means of sh-*Kif3a*-GFP slightly enhanced the cell cycle re-entry in NIH3T3^{WT} cells, consistent with previous findings seen upon *Ift88* knockdown (Kim et al., 2011). To our surprise, sh-*Kif3a*-GFP restores the delay of cell cycle re-entry in NIH3T3$^{Gli2-/-}$ cells after serum re-stimulation for 16 and 24 h (Fig. 6B,C). Taken together, these results demonstrate that the elongated primary cilium is responsible for the delay in cell cycle re-entry in NIH3T3$^{Gli2-/-}$ cells.

DISCUSSION

In this study, we established the first Gli2-knockout fibroblast cell line using CRISPR/Cas9 technology (Fig. 1), which has become popular for cilia studies in different organisms (Breslow et al., 2018; Katoh et al., 2017; Li et al., 2015; Pusapati et al., 2018). We showed that both depletion and knockout of Gli2 expression increased primary cilia length after serum starvation (Fig. 2; Fig. S2C). Mechanistically, we found that the autophagy flux was increased in association with a decrease in Ofd1 in NIH3T3$^{Gli2-/-}$ cells after serum starvation (Fig. 3; Fig. S3). Interestingly, pharmacological and genetic inhibition of autophagy, through 3-MA and sh-*Atg3*-GFP, respectively, rescued the Ofd1 protein level (Fig. S5) and alleviated the effect of growing longer primary cilia in NIH3T3$^{Gli2-/-}$ cells (Fig. 4). In addition, NIH3T3$^{Gli2-/-}$ cells showed a slower ciliary resorption (Fig. 5) and cell cycle re-entry after serum add-back; inhibition of ciliogenesis by means of Kif3a knockdown reversed this effect (Fig. 6). These results indicate that Gli2 regulates autophagy-mediated Ofd1 removal to control primary cilia formation and cell cycle progression in fibroblasts (Fig. 7).

Gli2 utilizes autophagy to control ciliary length

Our work identified Gli2 as a negative regulator for ciliary length, which is controlled through a balance between ciliary assembly and disassembly. Recent studies have shown that ciliary length can be regulated by proteins that mediate ciliary disassembly, including Nek2–Kif24, Aurora kinase A–HDAC6, and Nde1 (Kim et al., 2015, 2011; Maskey et al., 2015; Pugacheva et al., 2007). In addition, several proteins, such as dynein heavy chain-2 (DHC2, also known as DYNC2H1), dynein light chain Tctex-1 (also known as DYNLT1), and the centriolar protein calcineurin-2, are responsible for cilia length regulation (Palmer et al., 2011; Stevenson et al., 2018). On the other hand, several negative regulators for ciliogenesis, such as the APC-Cdc20 and Ofd1, have been reported to modulate the length of primary cilia (Tang et al., 2013; Wang et al., 2014). Upon serum starvation, Ofd1 is removed from centriolar satellites by autophagy via an integration with LC3, which allows the initiation of ciliary growth. Here, we found that Gli2 knockout enhanced the activation of autophagy required for Ofd1 removal during ciliogenesis (Fig. 3; Fig. S3). Importantly, we showed that inhibition of autophagy restored the primary cilia length and Ofd1 protein level in Gli2-knockout cells (Fig. 4; Fig. S5), suggesting that Gli2 regulates ciliary elongation, at least in part, through the autophagy pathway. Interestingly, although the inhibition of autophagy significantly reduced the ciliary length in NIH3T3$^{Gli2-/-}$ cells, the average ciliary length was still slightly longer than that in control cells treated with autophagy inhibitors (Fig. 4), suggesting that additional mechanisms may participate downstream of Gli2 for regulating ciliary length. Our findings specifically link Gli2-dependent ciliary length control to the autophagy-mediated Ofd1 removal.

The interplay between Gli2 and autophagy

In this paper, we found that Gli2 depletion in NIH3T3 fibroblasts enhanced autophagic flux (Fig. 3; Fig. S3), possibly due to the reduction of Gli transcriptional activities as shown in the Gli reporter assay (Fig. 1C). This finding is consistent with previous findings with manipulations of SHH and Gli activities in several other systems. In cancer cells, inhibition of the SHH signaling pathway hinders their proliferation, in part through upregulation of autophagy (Tang et al., 2015). In pancreatic ductal adenocarcinoma cells, activation of SHH signaling inhibits autophagy, whereas pharmacological inhibition of Gli1 and Gli2, induces autophagy (Xu et al., 2014). Interestingly, not only serum starvation but also Gli2 mediates the SHH-dependent

Journal of Cell Science (2018) 131, jcs221218. doi:10.1242/jcs.221218

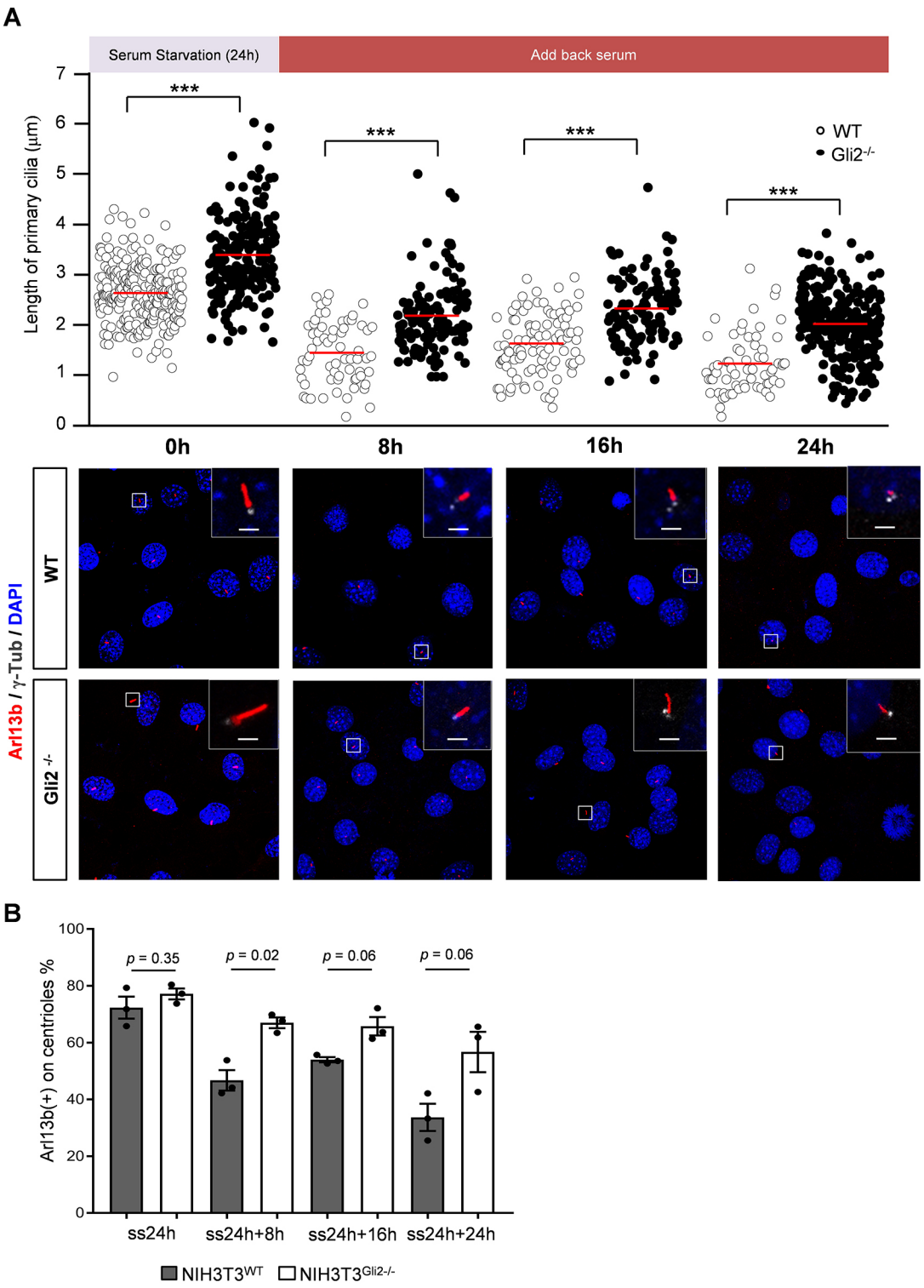

Fig. 5. Delay in ciliary resorption in NIH3T3$^{Gli2-/-}$ cells. (A) Time course of ciliary length in NIH3T3 cells after serum re-stimulation. The primary cilium (red, Arl13b), centrioles (gray, γ-tubulin) and nuclei (DAPI) in NIH3T3^{WT} and NIH3T3$^{Gli2-/-}$ cells were stained after serum re-supplementation for 0, 8, 16, and 24 h following 24 h of serum starvation. The scatter plots display individual cilia in NIH3T3^{WT} cells (white circles) and NIH3T3$^{Gli2-/-}$ cells (black dots). Red lines mark the mean. Insets represent the boxed region in each panel. Scale bars: 2 µm. NIH3T3^{WT} at 0 h, *n*=269; 8 h, *n*=64; 16 h, *n*=95; 24 h, *n*=64; NIH3T3$^{Gli2-/-}$ at 0 h, *n*=196; 8 h, *n*=113; 16 h, *n*=113; 24 h, *n*=261. ***P<0.001 (Mann–Whitney *U*-test). (B) Bar graph along with individual data points representing the percentage of centrioles possessing an Arl13b-positive signal (indicating that the primary cilium is present on the centrioles) after serum starvation for 24 h (ss24), followed by serum re-stimulation for indicated conditions (+8h, +16h, +24h). *n*=3 trials. *P*-values are shown (Student's *t*-test).

regulation of autophagy seen upon rapamycin treatment or trehalose induction (Jimenez-Sanchez et al., 2012). This regulation was likely meditated by the autophagy modulator, PERK (also known as EIF2AK3), an ER-resident protein responsible for the phosphorylation of eukaryotic initiation factor 2 α (EIF2α), leading to the inhibition of protein translation in response to ER stress

Journal of Cell Science (2018) 131, jcs221218. doi:10.1242/jcs.221218

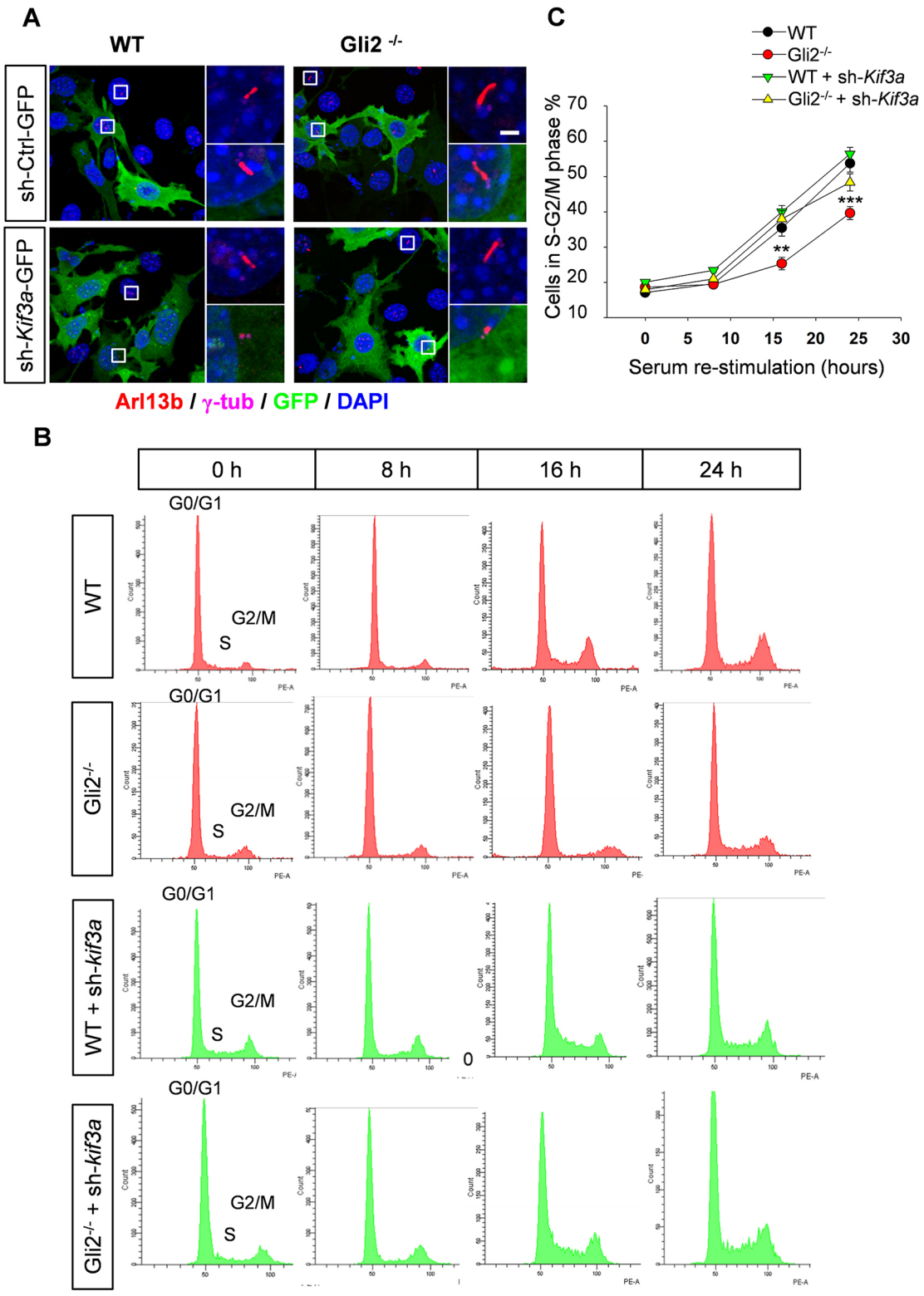

Fig. 6. Ablation of the primary cilia by Kif3a knockdown rescues the delay of cell cycle re-entry in NIH3T3$^{Gli2-/-}$ cells. (A) Immunostaining of the primary cilia (Arl13b, red), centrioles (γ-tubulin, magenta) and nucleus (DAPI, blue) in NIH3T3^{WT} and NIH3T3$^{Gli2-/-}$ cells transfected with sh-Ctrl-GFP or sh-*Kif3a*-GFP (green). The boxed regions are magnified in right of each panel, and show the primary cilia in non-transfected cells (GFP−; top) and transfected cells (GFP+; bottom). *Kif3a* shRNA effectively eliminates the growth of primary cilia in both NIH3T3^{WT} and NIH3T3$^{Gli2-/-}$ cells. Scale bar: 2 µm. (B) Cell cycle analysis by flow cytometry in NIH3T3^{WT} and NIH3T3$^{Gli2-/-}$ cells and cells transfected with sh-Ctrl-GFP or sh-*Kif3a*-GFP. Cells were synchronized via serum starvation for 24 h and then collected for 0 h, 8 h, 16 h, and 24 h after serum re-stimulation. (C) The line chart shows the time course of cell cycle re-entry after 0 h, 8 h, 16 h, and 24 h of serum add-back in NIH3T3^{WT} cells and NIH3T3$^{Gli2-/-}$ cells transfected with either sh-Ctrl-GFP or sh-*Kif3a*-GFP. *n*=3 trials. While NIH3T3$^{Gli2-/-}$ cells showed a delay in cell cycle re-entry, *Kif3a* shRNA rescued this effect. ***P*<0.01, ****P*<0.001 (one-way ANOVA with post-hoc Bonferroni test).

Journal of Cell Science (2018) 131, jcs221218. doi:10.1242/jcs.221218

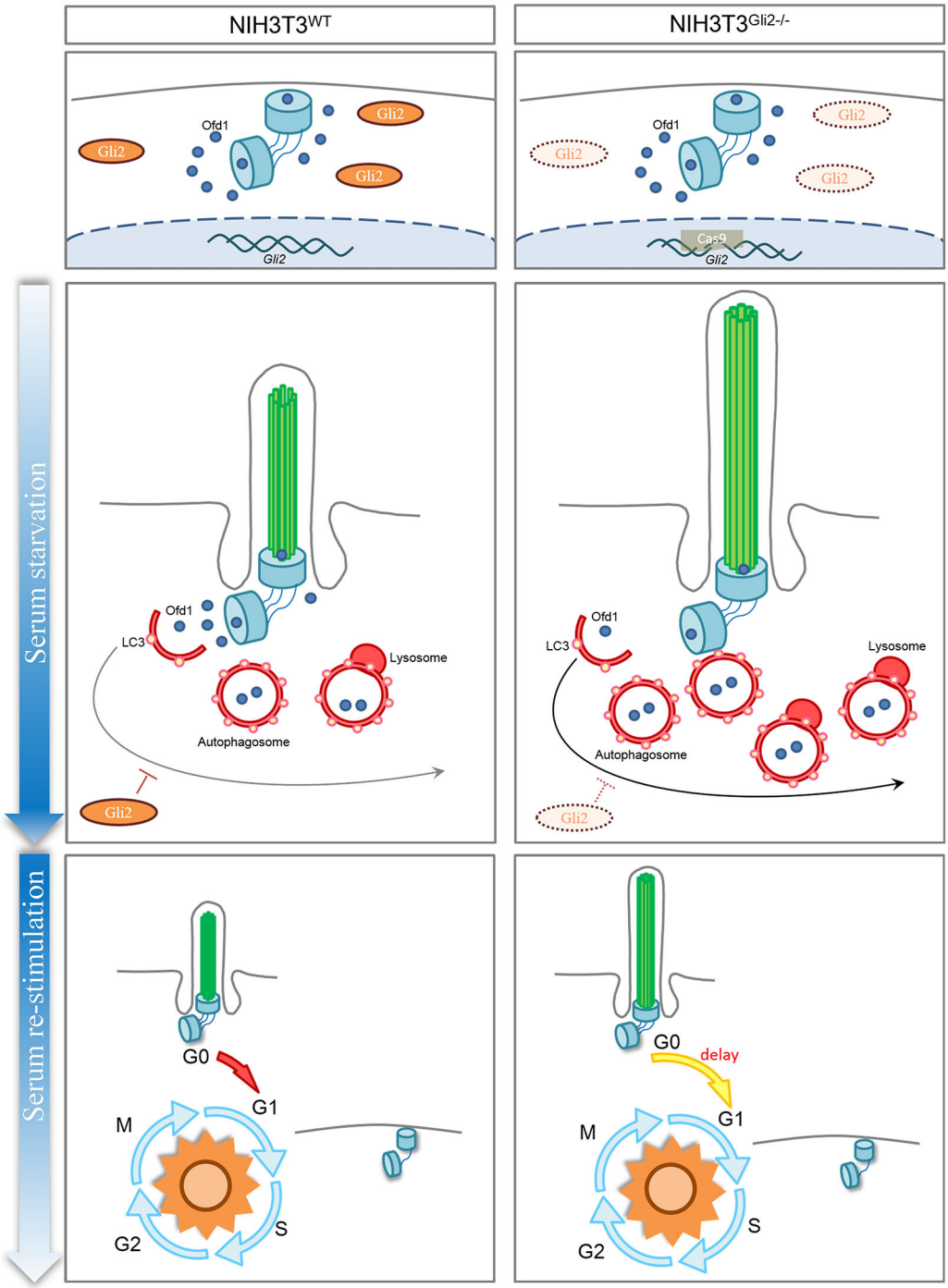

Fig. 7. Proposed model for the relationship between Gli2 and primary cilia-dependent cell cycle re-entry. In NIH3T3^{WT} cells, the presence of Gli2 represses the progression of autophagy, which reduces the autophagy-dependent Ofd1 removal during serum starvation. In NIH3T3$^{Gli2-/-}$ cells, loss of Gli2 releases the inhibition of autophagy, leading to more Ofd1 removal upon serum starvation. This process contributes to the elongation of ciliary length, resulting in the delay of cell cycle re-entry after serum re-stimulation.

(Jimenez-Sanchez et al., 2012). Here, we confirmed that the expression of *Perk* was highly elevated in NIH3T3$^{Gli2-/-}$ cells upon serum starvation for 24 h by quantitative real-time RT-PCR (RT-qPCR) (Fig. S7A). Accumulating data implies that PERK may negatively regulate the mammalian target of rapamycin (mTOR) activity, leading to the activation of autophagy (Bobrovnikova-Marjon et al., 2012; Qin et al., 2010). Consistent with this, we found that the protein level of phosphorylated S6 ribosomal protein (p-S6) was decreased in NIH3T3$^{Gli2-/-}$ cells compared to the level in NIH3T3$^{Gli2-/-}$ cells, whereas the expression of S6 was the same in both cells, suggesting that the mTOR activity is be reduced in NIH3T3$^{Gli2-/-}$ cells (Fig. S7B). Therefore, our findings of Gli2 regulation of autophagy is well in line with previous studies.

The role of Gli2 on cell cycle re-entry and ciliary elongation

Here, we also showed that Gli2 depletion leads to late cell cycle re-entry while the ablation of primary cilia restores the cell cycle re-entry in NIH3T3$^{Gli2-/-}$ cells (Fig. 6). Gli2 is known to regulate

the cell cycle through the canonical Hh signaling pathway by elevating cyclin D, which is required for cell cycle progression at G0/G1 (Katoh and Katoh, 2009). For decades, it has been well characterized that cyclin D is crucial for G1/S progression by binding to CDK4 and CDK6, two cyclin-dependent kinases which phosphorylate retinoblastoma (Rb) protein, and thus release the inhibition of E2F transcription factors, which are necessary for driving genes required for G1/S transition (Bertoli et al., 2013).

Interestingly, not only the Gli transcription factors, but also the primary cilia are tightly correlated with cell cycle progression. The assembly of the primary cilium usually occurs during G1/G0 phase; after that, the primary cilium rapidly becomes shorter as cells progress from G1 to S phase through the activation of Plk1 and Aurora A kinase activity, indicating that ciliary disassembly coincides with cell cycle re-entry (Fu et al., 2015; Izawa et al., 2015; Kim and Tsiokas, 2011; Pugacheva et al., 2007). The presence of primary cilia, especially a longer primary cilia functions as a brake for cell cycle re-entry (Kim et al., 2011; Li et al., 2011). For example, cells depleted of Nde1 possess longer cilia, which is responsible for the delay in cell cycle re-entry (Kim et al., 2011). In addition, overexpression a phospho-mimetic Tctex-1 (T94E), a negative ciliary regulator recruited to the transition zone during ciliary disassembly, leads to more cells re-entering to S-phase (Li et al., 2011). All these findings suggest that the primary cilium plays a critical role in cell cycle regulation.

Notably, as our experiments were conducted in medium without exogenous SHH, we did not see any significant difference in the phase of cell cycle distribution in NIH3T3^{WT} cells and NIH3T3$^{Gli2-/-}$ cells under nutrient-rich conditions (Fig. S6A). However, when serum re-stimulation was performed after cells were synchronized in G0/G1 phase, cells with Gli2 depletion showed a delay in cell cycle re-entry, suggesting that Gli2 plays a specific role in delaying cell cycle re-entry but not cell cycle progression in general (Fig. 6B,C). Importantly, ablation of the primary cilium through Kif3a knockdown restored this process, implying that the primary cilium mediates the delay of cell cycle re-entry in NIH3T3$^{Gli2-/-}$ cells (Fig. 6A,C). Therefore, in addition to the regulation on cyclin D upon SHH activation, we demonstrate that Gli2 plays a new role in regulating the cell cycle through the primary cilium.

Taken together, our findings suggest that Gli2 can regulate ciliary length through modulating autophagy-mediated Ofd1 degradation. This pathway may in turn facilitate cell cycle re-entry of resting fibroblasts (Fig. 7).

MATERIALS AND METHODS

Plasmids

The shRNAs targeting *Gli2*, *Kif3a*, and *Atg3* were obtained from National RNAi Core Facility in Taiwan. The targeting sequences for RNA interference (RNAi) are sh-*Gli2*#1: 5′-CACCAACCCTTCAGACTATTA-3′, sh*Gli2*#2: 5′-TGTGGAGGACTGCCTACATAT-3′, sh-*Kif3a*-GFP: 5′-ATATTGGGC-CAGCAGATTATA-3′ (Chen et al., 2018), sh-*Atg3*-GFP: 5′-GTACAT-CACTTACGACAAATA-3′. pC2-Arl13b-GFP was a kind gift from Dr Olivier Ayrault at Institut Curie, France. pCEFLmGFP-Gli2 and pIRES2-eGFP-Ofd1-myc for Gli2 and Ofd1 overexpression were Addgene plasmid #37672 (deposited by Philip Beachy; Kim et al., 2009), Addgene plasmid #24560 (deposited by Jeremy Reiter; Singla et al., 2010), respectively. pUS2 and pUS2-Gli2 were generous gift from Dr Jenn-Yah Yu (Department of Life Sciences and Institute of Genome Sciences, Taipei City, Taiwan), who also provided the luciferase reporter constructs, 8×3′Gli-BS and 8×3′ mGli-BS (Lin et al., 2012), who received this plasmids from H. Sasaki (Sasaki et al., 1999). The promoter region for the luciferase reporter contains eight copies of wild-type Gli-binding motif (GAACACCCA); a mutant Gli-binding motif (GAAGTGGGA) served as a control.

Cell culture and transfection

NIH3T3 cells were obtained from ATCC (CRL-1658) and tested for contamination; thereafter, cells were maintained in Dulbecco's modified Eagle's medium (DMEM; Life Technologies), pH 7.3, supplemented with 10% calf serum, 1% 100 U/ml penicillin and 100 µg/ml streptomycin, and 1% L-glutamine at 37°C in humidified atmosphere with 5% CO_2 (Jheng et al., 2018). Cells were serum starved at the beginning of transfection in order to maintain cells in G0/G1 phase, which induces the growth of primary cilia. In experiments where autophagy was blocked, 3-methyladenine (10 mM, Sigma-Aldrich) was applied as previously described (Orhon et al., 2016). Plasmids were transfected into NIH3T3 cells via Lipofectamine 3000 reagent (Invitrogen) according to the manufacturer's recommended protocol. Primary cilia were observed by confocal microscopy (Zeiss LSM 700) after serum starvation and transfection.

CRISPR/Cas9 technology

To establish the Gli2-knockout cell line, we used CRISPR/Cas9 technology as previously described (Doudna and Charpentier, 2014). Briefly, we designed three different Gli2 sgRNAs (Gli2sgRNA#1, Gli2sgRNA#2, and Gli2sgRNA#3; Table S1), with the MIT CRISPR design tool (http://crispr.mit.edu/), that targeted the exon 2 region of the Gli2 gene. Next, we annealed two oligonucleotides in each sgRNA pair and extended them to make a 100 bp double-stranded DNA fragment by using Phusion polymerase (NEB). Subsequently, these double-stranded DNA fragments were inserted into the pCR-Blunt II-TOPO vector. NIH3T3 cells were transfected with pCP-Blunt II-TOPO-sgGli2 and Cas9 constructs by Lipofectamine 3000 (Invitrogen), followed by determination of the knockout efficiency through western blotting.

Single-cell selection

After transfection for 5 days with Gli2sgRNA#1 and Cas9 by Lipofectamone 3000 (Invitrogen), cells were selected and transferred to 96-well plates with 1 cell per well. Once these cells reached 60% confluency, they were sub-cultured into a single well of a 48-well plate. As these cells reached 80% confluence, we sub-cultured the cells into three 60 mm dishes for genomic DNA extraction and protein analysis.

Extraction of genomic DNA and sequencing

The collected cells were suspended in 500 µl lysis buffer (Goal Bio), followed by addition of 10 µl (20 mg/ml) proteinase K (BIOTOOLS) at 55°C for 1 h. Next, we purified the gDNA by using protein precipitation buffer (Goal Bio) according to the manufacturer's protocol. The primers for sequencing the Gli2 exon 2 are: forward, 5′-TATGAGCCTCTGAG-ATGGAG-3′ and reverse, 5′-ACAAGAAAGCATCAGAGCAC-3′.

Immunoblotting

Cells were washed in PBS and lysed in 1× RIPA buffer (50 mM Tris-HCl pH 8.0, 150 mM NaCl, 1% Nonidet P-40, 0.5% sodium deoxycholate, 0.1% SDS) with protease inhibitor cocktail (Sigma Aldrich) and phosphatase inhibitors (Roche). Lysates were sonicated in icy water and cleared by centrifugation (21,000 ***g*** for 15 min), and protein concentration was determined by using the Pierce BCA protein assay kit (Thermo Scientific), followed by electrophoresis on a 0.1% SDS, 40% acrylamide/bis-acrylamide gradient gel (TOOLS), and transfer onto a PVDF membrane (Millipore). Primary antibodies used were: rabbit anti-Gli2, 1:500 (Abcam, cat. no. ab167389); rabbit anti-LC3, 1:500 (Proteintech, cat. no. 14600-1-AP); rabbit anti-Ofd1, 1:500 (Abcam, cat. no. ab222837); rabbit anti-P62, 1:1000 (Proteintech, cat. no. 18420-1-AP); rabbit anti-phospho-S6 ribosomal protein, 1:1000 (Cell Signaling Technology, cat. no. #2211); rabbit anti-S6 ribosomal protein, 1:1000 (Cell Signaling Technology, cat. no. #2217); mouse anti-GAPDH, 1:10,000 (Proteintech, cat. no. 60004-1-Ig); mouse anti-β-actin, 1:10,000 (Proteintech, cat. no. 60008-1-Ig), and mouse anti-α-tubulin, 1:5000 (Proteintech, cat. no. 66031-1-Ig). Next, horseradish peroxidase (HRP)-conjugated secondary antibodies were applied as below: anti-rabbit-IgG (1:10,000, Sigma Aldrich), and anti-mouse-IgG (1:10,000, GeneTex). Signals were generated with ECL-Plus reagent (Millipore), and detected under the Luminescence/Fluorescence

Imaging System LAS-4000 (Fujifilm). Signal quantification was performed with Image-J software (NIH).

Luciferase reporter assay

NIH3T3^{WT} and NIH3T3$^{Gli2-/-}$ cells in 24-well plates were transfected with 0.025 µg US2-renilla Luciferase, and 0.3875 µg firefly luciferase with either normal or mutant Gli-binding sites as the promoters. Gli2 overexpression was achieved by transfecting 0.3875 µg of the pLKO-Gli2 construct whereas 0.3875 µg PLKO construct was used as control. The dual luciferase assay (Promega) was performed according to the manufacturer's protocol. The relative luciferase intensity is calculated as previously described (Lin et al., 2012): (GliBS firefly luciferase/*Renilla* luciferase in the same cells)/(mutant GliBS firefly/*Renilla* luciferase in the same cells).

Immunocytochemistry

NIH3T3^{WT} and NIH3T3$^{Gli2-/-}$ cells were plated on glass coverslips coated with 0.2 mg/ml poly-D-lysine (Sigma Aldrich) and ciliogenesis was induced by serum starvation for 24 h. The cells were then fixed for 15 min in 4% paraformaldehyde (PFA) at room temperate followed with cold methanol/acetone (1:1) for 5 min, washed in PBS and incubated in PBS with 0.2% Triton X-100 (PBST) for 15 min. The cells were blocked in 10% normal goat serum (NGS) and 5% bovine serum albumin (BSA) in PBS for 1 h at room temperature and were incubated overnight with primary antibody at 4°C. Primary antibodies were used at the following concentrations: mouse anti-Arl13b, 1:500 (NeuroMab, cat. no. 73-287); mouse anti-acetylated α-tubulin, 1:500 (Abcam, cat. no. ab24610); and rabbit anti-γ-tubulin, 1:1000 (Abcam, cat. no. ab11317); rabbit anti-Pcm1, 1:500 (Bethyl Laboratories, cat. no. A301-149A); rabbit anti-Ofd1, 1:500 (Abcam, cat. no. ab222837); rabbit anti-Myc tag (Proteintech, cat. no. 16286-1-AP). The cells were washed in PBS and incubated in secondary antibodies (conjugated to Alexa Fluor 488, 546, or 647, 1:500 for each antibody) for 2 h at room temperature. Finally, the coverslips were counterstained with 0.5 µg/ml DAPI (Invitrogen). VECTASHIELD® Mounting Medium Media (Vector Laboratories) was added before sealing the slides.

Flow cytometry

Flow cytometry (BD FACSCanto) was applied to observe cell cycle distribution of NIH3T3^{WT} and NIH3T3$^{Gli2-/-}$ cells. For analysis of the DNA content, cells were fixed with 0.5% formaldehyde and stored at −20°C for no longer than 24 h. After fixation, cells were stained with 20 µg/ml propidium iodide (PI, Sigma Aldrich) plus 200 µg/ml RNase A (Sigma Aldrich) in PBS and subjected to flow cytometry analysis. At least 10,000 cells were analyzed per sample.

RNA extraction and RT-qPCR

Total RNA extraction from NIH3T3 cells was performed with *Quick*-RNA™ MiniPrep (ZYMO RESEARCH) according to manufacturer's protocol. Removal of genomic DNA was achieved through DNase I treatment, as provided in the kit, and cDNA was synthesized by using the iScript™ cDNA Synthesis Kit (BIO-RAD) following the provider's instructions. RT-qPCR was performed with a OmicsGreen qPCR Master Mix (Omics Bio). Primers used in RT-qPCR for *Perk* expression were: forward: 5′-CACAGGGACCTCAAGCCTTC-3′; reverse: 5′-GTCCCTAC-TTGTCCCGTGTG-3′.

Microscopy

Glass coverslips were imaged under an inverted laser scanning confocal microscope (LSM-700, Zeiss). The excitation wavelengths were 647 nm for infrared, 546 for red fluorescence, 488 nm for EGFP, and 405 nm for DAPI. The *Z*-stack section was set for 0.1 µm for observation of primary cilia. Analysis of images were performed with Zen software (Zeiss) or ImageJ software (NIH).

Image analysis and fluorescence intensity quantification

The measurement of the LC3 puncta (Fig. 3B) was performed as previously described (Dupont et al., 2014; Yoshii and Mizushima, 2017). In brief, cells were transfected with plasmids encoding RFP–GFP–LC3 under basal (serum-rich) as well as serum-free conditions. Images were analyzed by using the ITCN plugin in ImageJ software. Individual puncta were measured and defined as one dot according to the instructions from Academic Technology at Keene State College (https://www.youtube.com/watch?v=PqHFsmS1_JY). To measure the density of the puncta, the number of dots were normalized to the total area in each cell. Next, the density of LC3 puncta upon serum starvation was further normalized to that under the basal condition for each group.

For measurement of Ofd1 intensity around the centrioles (related to Fig. S4C), both NIH3T3^{WT} and NIH3T3$^{Gli2-/-}$ cells stained with Ofd1 and γ-tubulin were imaged under the same criteria, followed by analysis using ImageJ. Centered on the γ-tubulin signal, we measured the signal intensity of Ofd1 within a circular area of 34.9 µm^2. Next, the signal intensity of Ofd1 in NIH3T3^{WT} cells was normalized to 1, and then the signal intensity of Ofd1 in NIH3T3$^{Gli2-/-}$ cells was calculated relative to that in NIH3T3^{WT} cells.

Statistical analysis

Statistical significance was determined with Excel and SPSS software. Two-tailed tests were performed and $P<0.05$ was considered as statistical significant. Data are shown as mean±s.e.m. or s.d. as indicated in figure legends. Bar graphs were drawn with Excel (Microsoft) and Prism (GraphPad) software. When the sample number was less than five, bar graphs along with individual data point are shown.

Acknowledgements

We thank Dr Feng Zhang at MIT for providing a platform for optimized CRISPR designs. We also thank Pei-Jun Hsen, and Yung-Yu Lu for confocal imaging assistance. We especially thank Dr Olivier Ayrault (pC2-Arl13b-GFP), Jenn-Yah Yu (Gli-luciferase vectors) and the National RNAi core of Taiwan for providing plasmids.

Competing interests

The authors declare no competing or financial interests.

Author contributions

Conceptualization: C.H., C.C., W.W., J.T.; Methodology: C.H., C.C., R.B.I., I.L., C.W., W.W., J.T.; Validation: C.H., C.C., R.B.I., I.L., C.W., W.W.; Formal analysis: C.H., C.C., R.B.I., C.W., W.W., J.T.; Investigation: C.H., C.C., R.B.I., I.L., C.W., W.W.; Data curation: C.H., C.C., C.W., J.T.; Writing - original draft: C.H., C.C., J.T.; Writing - review & editing: C.H., C.C., R.B.I., I.L., C.W., W.W., J.T.; Visualization: C.H., C.C., J.T.; Supervision: W.W., J.T.; Project administration: J.T.; Funding acquisition: J.T.

Funding

This work was funded by Ministry of Science and Technology, Taiwan (MOST-103-2911-I-010-504, 103-2628-B-010-002-MY3, 101-2320-B-010-077-MY2, 104-2633-H-010-001, 105-2633-B-009-003, 106-2628-B-010-002-MY3, 106-2911-I-010-508, 107-2628-B-010-002-MY3, 107-2221-E-010-014, and 107-2321-B-075-001), National Health Research Institutes, Taiwan (NHRI-EX103-10314NC), and Academia Sinica, Taiwan (AS-104-TP-B09) to J.-W.T.; and MOST 105-2628-B-010-004-MY3, MOST 107-2313-B-010-001, and MOST107-2633-B-009-003 to W.-J.W. This work is also supported by the Development and Construction Program of NYMU School of Medicine (107F-M01-0502), and Brain Research Center, NYMU through the Featured Areas Research Center Program within the framework of the Higher Education Sprout Project by the Ministry of Education (MOE), Taiwan.

Supplementary information

Supplementary information available online at
http://jcs.biologists.org/lookup/doi/10.1242/jcs.221218.supplemental

References

Bertoli, C., Skotheim, J. M. and de Bruin, R. A. M. (2013). Control of cell cycle transcription during G1 and S phases. *Nat. Rev. Mol. Cell Biol.* **14**, 518-528.

Bobrovnikova-Marjon, E., Pytel, D., Riese, M. J., Vaites, L. P., Singh, N., Koretzky, G. A., Witze, E. S. and Diehl, J. A. (2012). PERK utilizes intrinsic lipid kinase activity to generate phosphatidic acid, mediate Akt activation, and promote adipocyte differentiation. *Mol. Cell. Biol.* **32**, 2268-2278.

Breslow, D. K., Hoogendoorn, S., Kopp, A. R., Morgens, D. W., Vu, B. K., Kennedy, M. C., Han, K., Li, A., Hess, G. T., Bassik, M. C. et al. (2018). A CRISPR-based screen for Hedgehog signaling provides insights into ciliary function and ciliopathies. *Nat. Genet.* **50**, 460-471.

Chen, J. L., Chang, C. H. and Tsai, J. W. (2018). Gli2 rescues delays in brain development induced by Kif3a dysfunction. *Cereb. Cortex*. doi: 10.1093/cercor/bhx356.
Craige, B., Tsao, C.-C., Diener, D. R., Hou, Y., Lechtreck, K.-F., Rosenbaum, J. L. and Witman, G. B. (2010). CEP290 tethers flagellar transition zone microtubules to the membrane and regulates flagellar protein content. *J. Cell Biol.* **190**, 927-940.
Doudna, J. A. and Charpentier, E. (2014). Genome editing. The new frontier of genome engineering with CRISPR-Cas9. *Science* **346**, 1258096.
Dupont, N., Orhon, I., Bauvy, C. and Codogno, P. (2014). Autophagy and autophagic flux in tumor cells. *Methods Enzymol.* **543**, 73-88.
Fu, J., Hagan, I. M. and Glover, D. M. (2015). The centrosome and its duplication cycle. *Cold Spring Harb. Perspect. Biol.* **7**, a015800.
Goetz, S. C. and Anderson, K. V. (2010). The primary cilium: a signalling centre during vertebrate development. *Nat. Rev. Genet.* **11**, 331-344.
Graser, S., Stierhof, Y.-D., Lavoie, S. B., Gassner, O. S., Lamla, S., Le Clech, M. and Nigg, E. A. (2007). Cep164, a novel centriole appendage protein required for primary cilium formation. *J. Cell Biol.* **179**, 321-330.
Haycraft, C. J. (2005). Gli2 and Gli3 Localize to Cilia and Require the Intraflagellar Transport Protein Polaris for Processing and Function. *PLoS Genet.* **1**, e53.
Izawa, I., Goto, H., Kasahara, K. and Inagaki, M. (2015). Current topics of functional links between primary cilia and cell cycle. *Cilia* **4**, 12.
Jheng, G.-W., Hur, S. S., Chang, C.-M., Wu, C.-C., Cheng, J.-S., Lee, H.-H., Chung, B.-C., Wang, Y.-K., Lin, K.-H., del Álamo, J. C. et al. (2018). Lis1 dysfunction leads to traction force reduction and cytoskeletal disorganization during cell migration. *Biochem. Biophys. Res. Commun.* **497**, 869-875.
Jimenez-Sanchez, M., Menzies, F. M., Chang, Y.-Y., Simecek, N., Neufeld, T. P. and Rubinsztein, D. C. (2012). The Hedgehog signalling pathway regulates autophagy. *Nat. Commun.* **3**, 1200.
Katoh, Y. and Katoh, M. (2009). Hedgehog target genes: mechanisms of carcinogenesis induced by aberrant hedgehog signaling activation. *Curr. Mol. Med.* **9**, 873-886.
Katoh, Y., Michisaka, S., Nozaki, S., Funabashi, T., Hirano, T., Takei, R. and Nakayama, K. (2017). Practical method for targeted disruption of cilia-related genes by using CRISPR/Cas9-mediated, homology-independent knock-in system. *Mol. Biol. Cell* **28**, 898-906.
Kim, S. and Tsiokas, L. (2011). Cilia and cell cycle re-entry: more than a coincidence. *Cell Cycle* **10**, 2683-2690.
Kim, J., Kato, M. and Beachy, P. A. (2009). Gli2 trafficking links Hedgehog-dependent activation of Smoothened in the primary cilium to transcriptional activation in the nucleus. *Proc. Natl. Acad. Sci. USA* **106**, 21666-21671.
Kim, S., Zaghloul, N. A., Bubenshchikova, E., Oh, E. C., Rankin, S., Katsanis, N., Obara, T. and Tsiokas, L. (2011). Nde1-mediated inhibition of ciliogenesis affects cell cycle re-entry. *Nat. Cell Biol.* **13**, 351-360.
Kim, S., Lee, K., Choi, J.-H., Ringstad, N. and Dynlacht, B. D. (2015). Nek2 activation of Kif24 ensures cilium disassembly during the cell cycle. *Nat. Commun.* **6**, 8087.
Lee, J. E. and Gleeson, J. G. (2011). A systems-biology approach to understanding the ciliopathy disorders. *Genome Med.* **3**, 59.
Li, A., Saito, M., Chuang, J.-Z., Tseng, Y.-Y., Dedesma, C., Tomizawa, K., Kaitsuka, T. and Sung, C.-H. (2011). Ciliary transition zone activation of phosphorylated Tctex-1 controls ciliary resorption, S-phase entry and fate of neural progenitors. *Nat. Cell Biol.* **13**, 402-411.
Li, W., Yi, P. and Ou, G. (2015). Somatic CRISPR–Cas9-induced mutations reveal roles of embryonically essential dynein chains in Caenorhabditis elegans cilia. *J. Cell Biol.* **208**, 683-692.
Lin, Y.-T., Ding, J.-Y., Li, M.-Y., Yeh, T.-S., Wang, T.-W. and Yu, J.-Y. (2012). YAP regulates neuronal differentiation through Sonic hedgehog signaling pathway. *Exp. Cell Res.* **318**, 1877-1888.
Lu, Q., Insinna, C., Ott, C., Stauffer, J., Pintado, P. A., Rahajeng, J., Baxa, U., Walia, V., Cuenca, A., Hwang, Y.-S. et al. (2015). Early steps in primary cilium assembly require EHD1/EHD3-dependent ciliary vesicle formation. *Nat. Cell Biol.* **17**, 531.
Maskey, D., Marlin, M. C., Kim, S., Kim, S., Ong, E.-C., Li, G. and Tsiokas, L. (2015). Cell cycle-dependent ubiquitylation and destruction of NDE1 by CDK5-FBW7 regulates ciliary length. *EMBO J.* **34**, 2424-2440.
Mizushima, N. and Komatsu, M. (2011). Autophagy: renovation of cells and tissues. *Cell* **147**, 728-741.
Orhon, I., Dupont, N., Zaidan, M., Boitez, V., Burtin, M., Schmitt, A., Capiod, T., Viau, A., Beau, I., Kuehn, E. W. et al. (2016). Primary-cilium-dependent autophagy controls epithelial cell volume in response to fluid flow. *Nat. Cell Biol.* **18**, 657-667.
Ott, C., Nachmias, D., Adar, S., Jarnik, M., Sherman, S., Birnbaum, R. Y., Lippincott-Schwartz, J. and Elia, N. (2018). VPS4 is a dynamic component of the centrosome that regulates centrosome localization of gamma-tubulin, centriolar satellite stability and ciliogenesis. *Sci. Rep.* **8**, 3353.
Palmer, K. J., MacCarthy-Morrogh, L., Smyllie, N. and Stephens, D. J. (2011). A role for Tctex-1 (DYNLT1) in controlling primary cilium length. *Eur. J. Cell Biol.* **90**, 865-871.
Pampliega, O., Orhon, I., Patel, B., Sridhar, S., Díaz-Carretero, A., Beau, I., Codogno, P., Satir, B. H., Satir, P. and Cuervo, A. M. (2013). Functional interaction between autophagy and ciliogenesis. *Nature* **502**, 194-200.
Pugacheva, E. N., Jablonski, S. A., Hartman, T. R., Henske, E. P. and Golemis, E. A. (2007). HEF1-dependent Aurora A activation induces disassembly of the primary cilium. *Cell* **129**, 1351-1363.
Pusapati, G. V., Kong, J. H., Patel, B. B., Krishnan, A., Sagner, A., Kinnebrew, M., Briscoe, J., Aravind, L. and Rohatgi, R. (2018). CRISPR screens uncover genes that regulate target cell sensitivity to the Morphogen sonic hedgehog. *Dev. Cell* **44**, 271.
Qin, L., Wang, Z., Tao, L. and Wang, Y. (2010). ER stress negatively regulates AKT/TSC/mTOR pathway to enhance autophagy. *Autophagy* **6**, 239-247.
Sahani, M. H., Itakura, E. and Mizushima, N. (2014). Expression of the autophagy substrate SQSTM1/p62 is restored during prolonged starvation depending on transcriptional upregulation and autophagy-derived amino acids. *Autophagy* **10**, 431-441.
Sasaki, H., Nishizaki, Y., Hui, C., Nakafuku, M. and Kondoh, H. (1999). Regulation of Gli2 and Gli3 activities by an amino-terminal repression domain: implication of Gli2 and Gli3 as primary mediators of Shh signaling. *Development* **126**, 3915-3924.
Shang, L., Chen, S., Du, F., Li, S., Zhao, L. and Wang, X. (2011). Nutrient starvation elicits an acute autophagic response mediated by Ulk1 dephosphorylation and its subsequent dissociation from AMPK. *Proc. Natl. Acad. Sci. USA* **108**, 4788-4793.
Singla, V., Hunkapiller, J., Santos, N., Seol, A. D., Norman, A. R., Wakenight, P., Skarnes, W. C. and Reiter, J. F. (2010). Floxin, a resource for genetically engineering mouse ESCs. *Nat. Methods* **7**, 50-52.
Stevenson, N. L., Bergen, D. J. M., Xu, A., Wyatt, E., Henry, F., McCaughey, J., Vuolo, L., Hammond, C. L. and Stephens, D. J. (2018). Regulator of calcineurin-2 is a centriolar protein with a role in cilia length control. *J. Cell Sci.* **131**, jcs212258.
Szymanska, K. and Johnson, C. A. (2012). The transition zone: an essential functional compartment of cilia. *Cilia* **1**, 10.
Tang, Z., Lin, M. G., Stowe, T. R., Chen, S., Zhu, M., Stearns, T., Franco, B. and Zhong, Q. (2013). Autophagy promotes primary ciliogenesis by removing OFD1 from centriolar satellites. *Nature* **502**, 254-257.
Tang, X., Deng, L., Chen, Q., Wang, Y., Xu, R., Shi, C., Shao, J., Hu, G., Gao, M., Rao, H. et al. (2015). Inhibition of Hedgehog signaling pathway impedes cancer cell proliferation by promotion of autophagy. *Eur. J. Cell Biol.* **94**, 223-233.
Tran, P. V., Sharma, M., Li, X. and Calvet, J. P. (2014). Developmental signaling: does it bridge the gap between cilia dysfunction and renal cystogenesis? *Birth Defects Res. C Embryo Today* **102**, 159-173.
Tsang, W. Y., Bossard, C., Khanna, H., Peränen, J., Swaroop, A., Malhotra, V. and Dynlacht, B. D. (2008). CP110 suppresses primary cilia formation through its interaction with CEP290, a protein deficient in human ciliary disease. *Dev. Cell* **15**, 187-197.
Varjosalo, M. and Taipale, J. (2008). Hedgehog: functions and mechanisms. *Genes Dev.* **22**, 2454-2472.
Wang, W., Wu, T. and Kirschner, M. W. (2014). The master cell cycle regulator APC-Cdc20 regulates ciliary length and disassembly of the primary cilium. *eLife* **3**, e03083.
Waters, A. M. and Beales, P. L. (2011). Ciliopathies: an expanding disease spectrum. *Pediatr. Nephrol.* **26**, 1039-1056.
Wheatley, D. N. (2005). Landmarks in the first hundred years of primary (9+0) cilium research. *Cell Biol. Int.* **29**, 333-339.
Williams, C. L., Li, C., Kida, K., Inglis, P. N., Mohan, S., Semenec, L., Bialas, N. J., Stupay, R. M., Chen, N., Blacque, O. E. et al. (2011). MKS and NPHP modules cooperate to establish basal body/transition zone membrane associations and ciliary gate function during ciliogenesis. *J. Cell Biol.* **192**, 1023-1041.
Xu, Y., An, Y., Wang, X., Zha, W. and Li, X. (2014). Inhibition of the Hedgehog pathway induces autophagy in pancreatic ductal adenocarcinoma cells. *Oncol. Rep.* **31**, 707-712.
Yoshii, S. R. and Mizushima, N. (2017). Monitoring and measuring autophagy. *Int. J. Mol. Sci.* **18**, 1865.

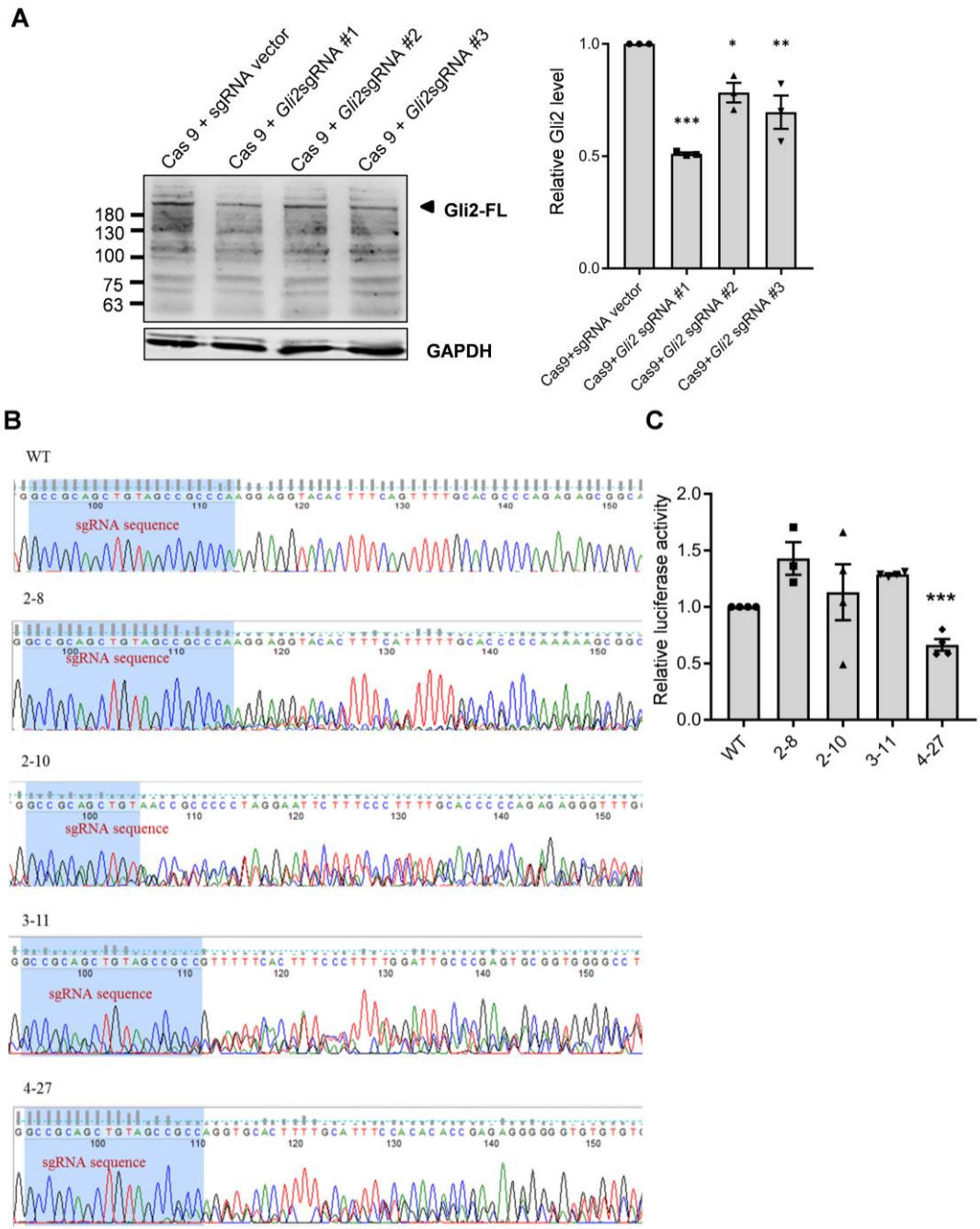

Figure S1. Selection and validation of ideal NIH3T3 clone for Gli2 knockout

(A) Protein lysates from NIH3T3 cells, transfected with Cas9 along with either sgRNA vector, Gli2sgRNA#1, Gli2sgRNA#2 or Gli2sgRNA#3, were immunoblotted for Gli2 or GAPDH (loading control). Bar graph along with individual data points represents the relative Gli2 protein level in each group (n = 3 trials). One-way ANOVA, post-hoc: Bonferroni test, *: $p<0.05$, **: $p<0.01$, ***: $p<0.001$.

(B) NIH3T3 cells were transfected with Gli2sgRNA#1 and Cas9, followed by expansion of 104 single cells for genomic DNA sequencing. Among them, clone #2-8, #2-10, #3-11, and #4-27 showed disruptions in the exon 2 portion of *Gli2* gene next to the sgRNA targeting sequence (blue).

(C) Gli-luciferase assay of the clone #2-8, #2-10, #3-11, and #4-27. Bar graph along with individual data points shows that the luciferase activity in clone #4-27 was significantly decreased compared to the wild type (n = 3 trials).

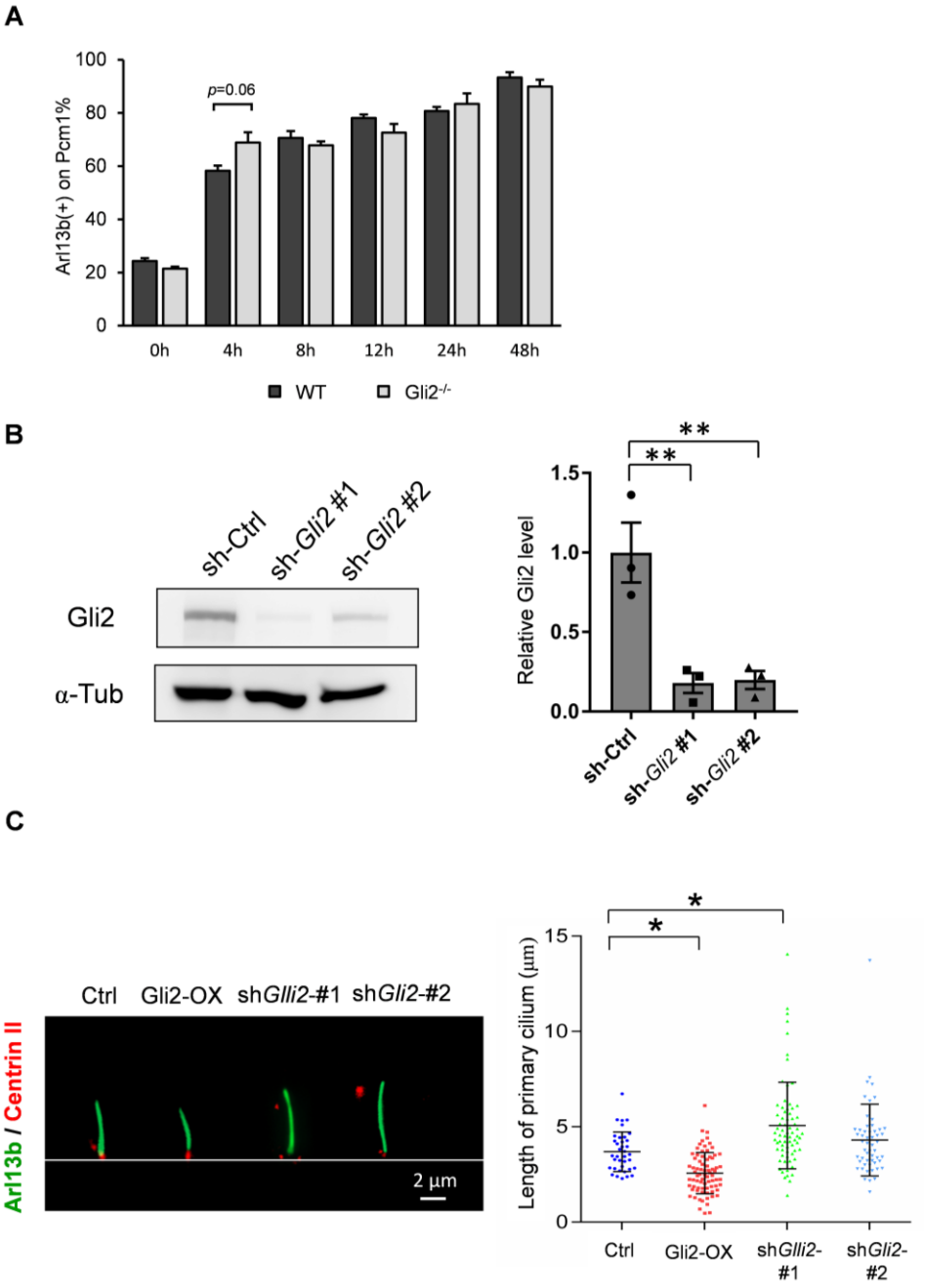

Figure S2. Percentage of ciliated cells and ciliary length in wild type and Gli2 depleted cells

(A) Statistics for the percentage of ciliated cells in NIH3T3^{WT} and NIH3T3$^{Gli2-/-}$ cells after serum starvation for indicated times. Bar graph exhibited that there is no difference between NIH3T3^{WT} cells and NIH3T3$^{Gli2-/-}$ cells possessing the primary cilium labelled by Arl13b. Cell were counted from 3 trials and cell numbers are listed as (WT, Gli2$^{-/-}$): 0hr (225, 299); 4hr (170, 179); 8hr (257, 333); 12hr (252, 281); 24hr (320, 313); 48hr (90, 93). Student's *t* test: $p>0.05$.

(B) Gli2 expression in NIH3T3 cells transfected with shRNAs. Protein lysates from NIH3T3 cells transfected with sh-Ctrl, sh-*Gli2* #1, and sh-*Gli2* #2 were immunoblotted with antibody against Gli2 and α-tubulin (α-Tub, loading control). Bar graph along with individual data points shows decreased Gli2 expression by both shRNAs (n = 3). One-way ANOVA, post-hoc: Bonferroni test, **: $p<0.01$.

(C) Examples of primary cilia in live NIH3T3 cells transfected with Gli2 overexpression or shRNA constructs after serum starvation for 24 hrs. PC2-Arl13bGFP (Green) and pmCherry-Centrin II (Red) were co-transfected to mark the primary cilia and basal bodies. Scatter plots shows that Gli2 knockdown by sh-*Gli2* #1 (n = 71 cells) or sh-*Gli2* #2 (n = 54 cells) increased the length of primary cilia compared to control cells (n = 37 cells), while Gli2-OX (n = 76 cells) slightly reduced the length of primary cilia. Kruskal Wallis test: $p<0.001$. Post-hoc: Mann-Whitney U test, *: $p<0.05$.

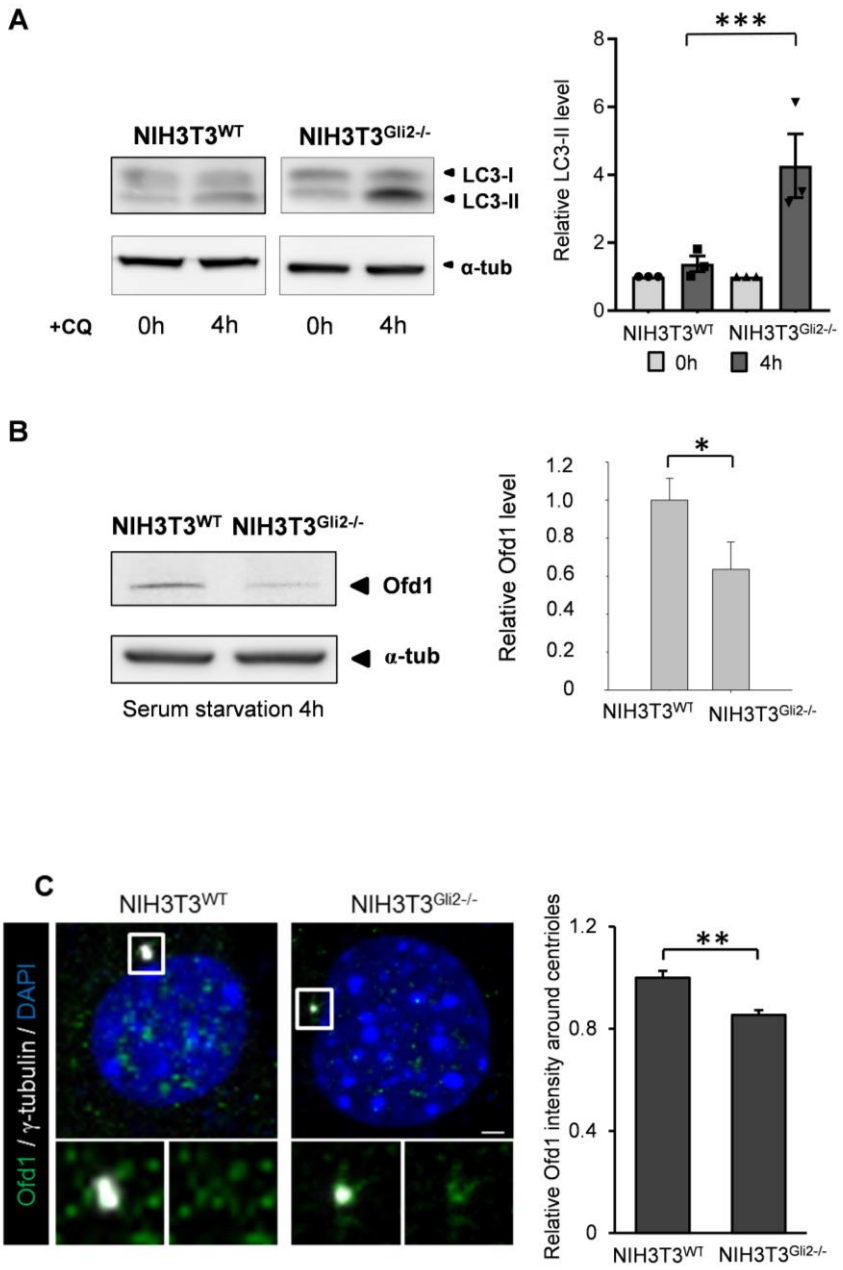

Figure S3. The induction of LC3-II and the reduction of Ofd1 in Gli2 knockout cells

(A) Protein lysates from NIH3T3^{WT} cells and NIH3T3$^{Gli2-/-}$ cells were treated with CQ for 0h and 4h under serum free condition, and then immunoblotted with antibody against LC3, and α-tubulin (α-tub, loading control). Bar graph along with individual data points exhibits the relative protein level of LC3-II at 4h compared to the basal condition (0h) in each group. N = 3 trials, Mann-Whitney *U* test, ***: $p<0.001$.

(B) Protein lysates were collected from NIH3T3^{WT} and NIH3T3$^{Gli2-/-}$ cells after serum starvation for 4h, and immunoblotted for Ofd1, and α-tub (loading control). Bar graph shows the relative protein levels of Ofd1 in NIH3T3$^{Gli2-/-}$ cells compared to WT cells; n = 6 trials, *: $p< 0.05$, student's *t* test.

(C) Immunostaining of Ofd1 satellites (Green) around the centrioles (γ-tubulin, white) in NIH3T3^{WT} cells and NIH3T3$^{Gli2-/-}$ cells after serum starvation for 24h. Boxed regions are enlarged in the bottom. Scale bar: 2μm. Bar graph shows the relative Ofd1 intensity surrounding the centrioles. NIH3T3^{WT}: n = 169 cells, NIH3T3$^{Gli2-/-}$: n = 127 cells. Mann-Whitney *U* test, **: $p<0.01$.

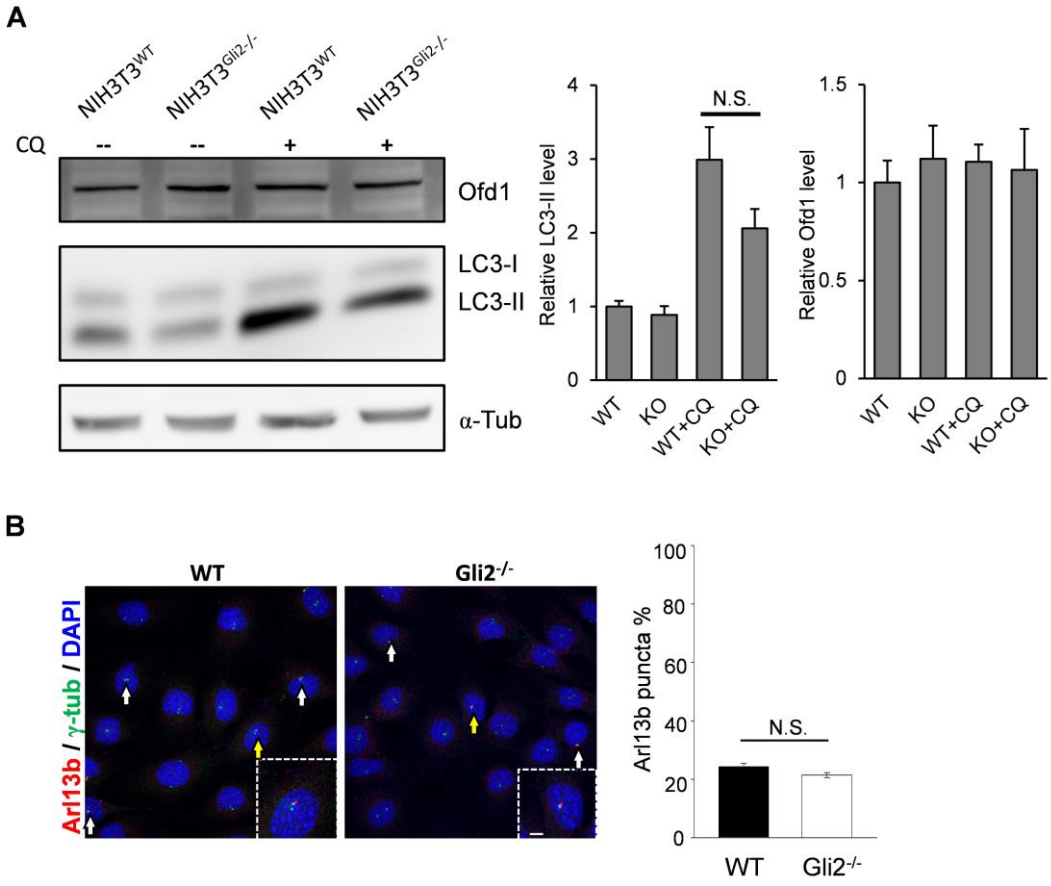

Figure S4. Comparable autophagy activity, Ofd1 protein level and percentage of primary cilium in Gli2 knockout cells under basal condition

(A) Protein lysates from NIH3T3^{WT} and NIH3T3$^{Gli2-/-}$ cells were treated with or without CQ for 4h under serum-rich condition, following by immunoblotting with antibody against Ofd1, LC3, and α-tubulin (α-tub, loading control). Bar graph displayed the relative protein level in each condition. n = 6 trials; ANOVA test, post-hoc: Bonferroni test.

(B) Immunostaining of primary cilia (Arl13b, red), centrioles (γ-tubulin, green) and DAPI (blue) under serum-rich condition. Arl13b+ puncta (arrows) were seldom detectable in both NIH3T3^{WT} and NIH3T3$^{Gli2-/-}$ cells. Centrioles pointed by the yellow arrows were magnified in the inlets. Scale bar: 5μm. Bar graph represents the percentage of centrioles possessing the Arl13b+ puncta. N = 225 in NIH3T3^{WT} cells, N = 299 in NIH3T3$^{Gli2-/-}$ cells; student's *t* test, $p>0.05$.

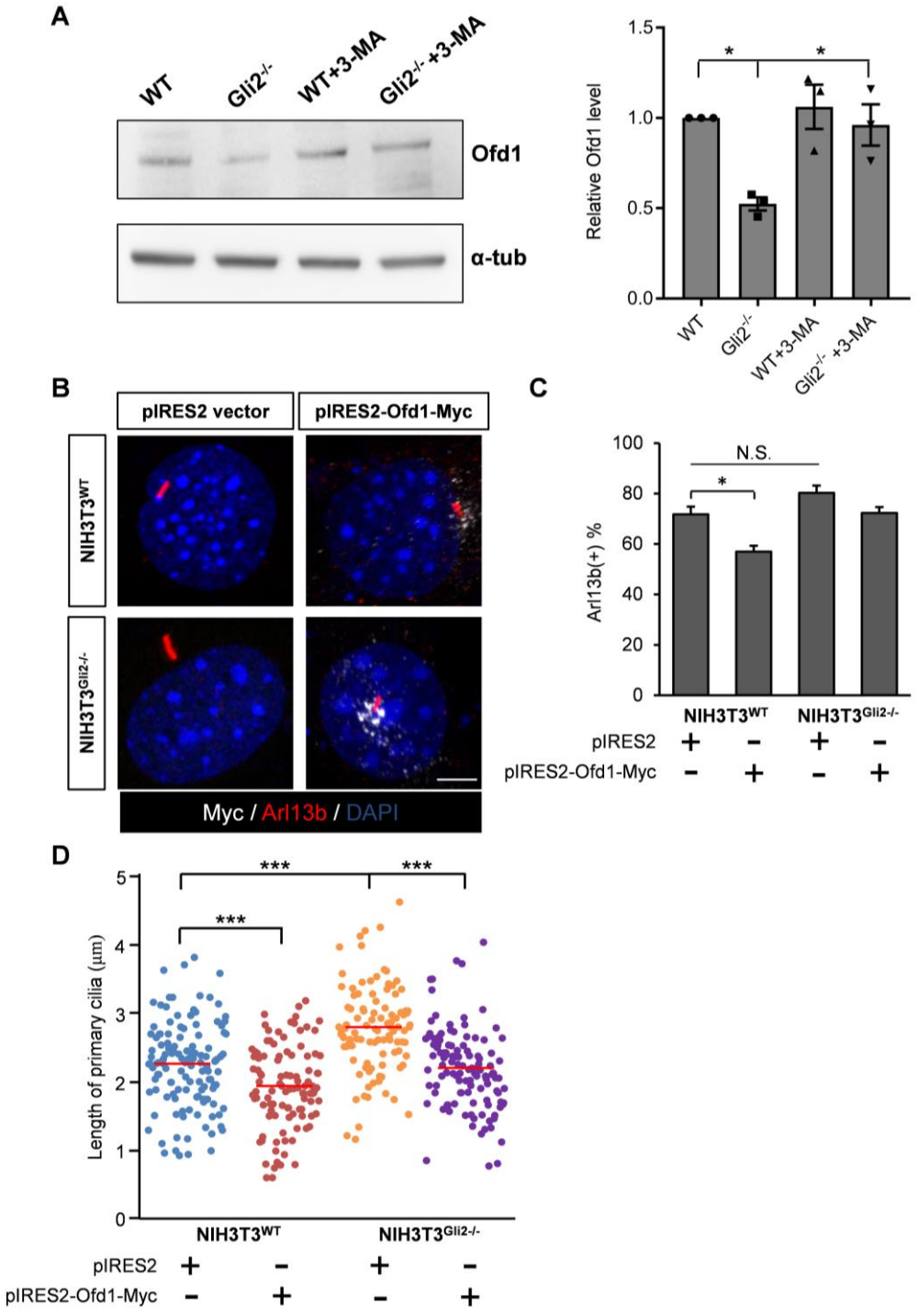

Figure S5. Rescue effect of Ofd1 reduction and ciliary elongation in Gli2 knockout cells treated with autophagy inhibitors and Ofd1 overexpression

(A) Protein lysates from NIH3T3^{WT} cells and NIH3T3$^{Gli2-/-}$ cells treated with or without 3-MA during serum starvation for 4h, were immunoblotted with antibodies against Ofd1 and α-tubulin. Bar graph along with individual data points represents the relative Ofd1 protein level in each condition. $n = 3$, ANOVA: $p = 0.008$; post-hoc: Bonferroni test, *: $p<0.05$.

(B) Immunostaining of Arl13b (red), myc-tag (Gray) and DAPI (blue) in NIH3T3^{WT} and NIH3T3$^{Gli2-/-}$ cells transfected with either vector (pIRES2) or myc-tagged Ofd1 (pIRES2-Ofd1-Myc) and

serum starved for 24h. Expression of Ofd1 shortened the length of primary cilia. Scale bar: 5µm.

(C) Bar graph represents the percentage of ciliated cells in each group. number of cells (WT, Gli2$^{-/-}$) transfected with pIRES2 = (291, 182); with pIRES2-Ofd1-myc = (208, 214). ANOVA test, post-hoc: Bonferroni test, *: $p<0.05$.

(D) Scatter plot exhibits the length of individual primary cilium in each group. Red lines mark the mean. Expression of Ofd1-myc significantly reversed the lengthening of primary cilia in NIH3T3$^{Gli2-/-}$ cells. In NIH3T3^{WT} cells, n = 126 and 104 cilia for pIRES2 and pIRES2-Ofd1-myc respectively; meanwhile, n = 104 and 118 cilia for NIH3T3$^{Gli2-/-}$ cells transfected with pIRES2 and pIRES2-Ofd1-myc respectively. ANOVA test: $p<0.001$. Post-hoc: Bonferroni test, ***: $p<0.001$.

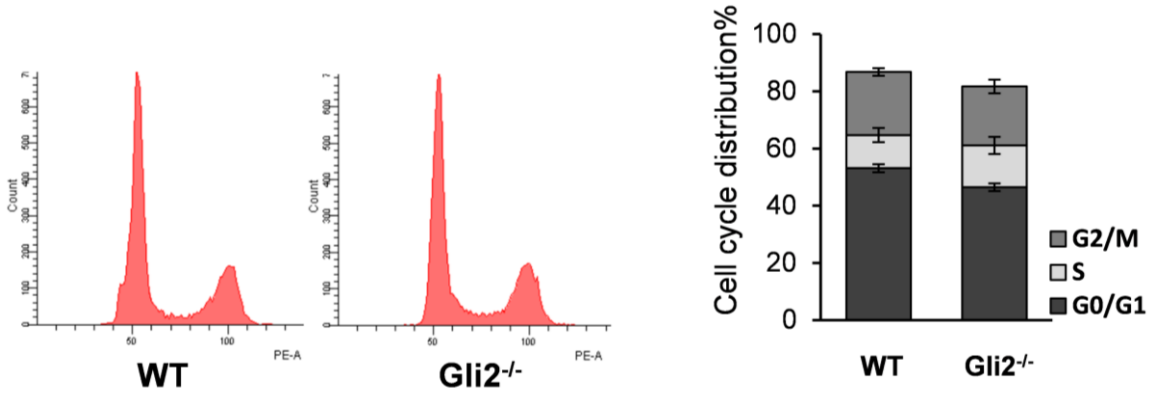

Figure S6. Gli2 knockout cells exhibit similar cell cycle distribution as wild type cells

Cell cycle analysis by flow cytometry in NIH3T3^{WT} and NIH3T3$^{Gli2-/-}$ cells for 24 hours after seeding. Bar graph indicates that the percentages of G0/G1, S and G2/M phases were not significant different between NIH3T3^{WT} and NIH3T3$^{Gli2-/-}$ cells (n = 3 trials). Student's *t* test, $p>0.05$.

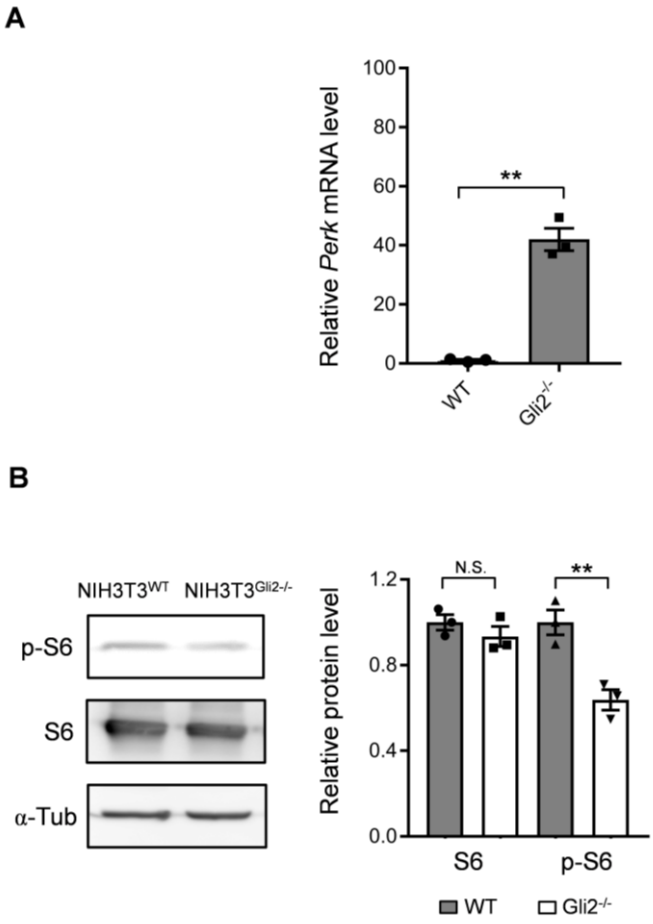

Figure S7. Potential mechanism in downstream of Gli2 for autophagy activation

(A) RT-qPCR for the expression of *Perk* mRNA upon serum starvation for 24h. Bar graph along with individual data points shows a significant increase in *Perk* mRNA in NIH3T3$^{Gli2-/-}$ cells compared to NIH3T3^{WT}. $n = 3$ trials. Student's t test, **: $p<0.01$.

(B) Protein lysates from NIH3T3^{WT} cells and NIH3T3$^{Gli2-/-}$ cells after serum starvation for 4h, and then immunoblotted with antibody against phospho-ribosomal protein S6 (p-S6), S6 and α-tubulin. Bar graph along with individual data points represents a significant decrease of the phosphorylation in S6 in NIH3T3$^{Gli2-/-}$ cells compared to NIH3T3^{WT} cells. $n = 3$ trials. Student's t test, **: $p<0.01$.

Table S1. Sequences for Gli2 guide RNA used in this study

No.	Direction	Sequence
*Gli2*sgRNA#1	Forward	TTTCTTGGCTTTATATATCTTGTGGAAAGGACGAAACA CCGCCGCAGCTGTAGCCGCCCA
	Reverse	GACTAGCCTTATTTTAACTTGCTATTTCTAGCTCTAAAA CTGGGCGGCTACAGCTGCGGC
*Gli2*sgRNA#2	Forward	TTTCTTGGCTTTATATATCTTGTGGAAAGGACGAAACA CCGTGCGGCCACCGCCAGAGGAC
	Reverse	GACTAGCCTTATTTTAACTTGCTATTTCTAGCTCTAAAA CGTCCTCTGGCGGTGGCCGCAC
*Gli2*sgRNA#3	Forward	TTTCTTGGCTTTATATATCTTGTGGAAAGGACGAAACA CCGACAGCAGCTTCCCCGACCC
	Reverse	GACTAGCCTTATTTTAACTTGCTATTTCTAGCTCTAAAA CGGGTCGGGGAAGCTGCTGTC

Table S2. Query coverage of candidate Gli2 KO lines.

NIH3T3 cell number	Query cover (%)
2-8	90%
2-10	99%
3-11	22%
4-27	10%